Chapter 4

NANOTUBES, IMAGING AND PROTEINS

An atomic force microscope can image the height (z) of a surface with extraordinary resolution. For a smooth surface it is relatively easy to achieve 0.25 Å in height resolution. However when the topography becomes more convoluted the detected height at any given point can be strongly influenced by the shape of the AFM probe. This becomes particularly apparent when determining the width of an object. The surface resolution (x-y) of an atomic force microscope is limited by the width of its tip (typically 5-10 nm radius).

The advantages of nanotube AFM probes are that they are very small in diameter and that the sides are vertical. As a result nanotube probes offer the potential for AFM imaging surface topography with minimal distortion due to the shape and size of the probe. Therefore we developed, in collaboration with the Pat Collier group, the capability to fabricate nanotube Atomic Force Microscope (AFM) probes.[1] In this paper we present how to grow nanotube substrates and fabricate nanotube AFM probes. As part of this effort we characterized the diameter of the nanotubes on the substrate. We also examine the resolution that nanotube AFM probes could achieve.

To our surprise we found that images taken with nanotube probes frequently demonstrated resolution better than could be expected given the apparent diameter of the nanotubes that were grown on the substrates that we used to supply nanotubes for attachment.

Therefore we (in an effort primarily conducted by Santiago Solaris of the Goddard group) used atomistic modeling to study the balance of forces that enabled nanotube attachment.[2] As a result of this effort we gained real insight into the basis for the surprisingly high imaging resolution we achieved with nanotube AFM probes.

Both of the papers referenced above are included in this chapter, along with their supporting material, courtesy of the American Chemical Society to whom they are copyrighted.

A US patent issued for the methods we invented for nanotube tip attachment to an AFM probe is included in Appendix G.[3] Appendix H is a patent[4] that describes a method of functionalizing nanotube tips. Specifically, it describes methods for coating the nanotube tipped probe to preclude non-specific binding or other chemical interactions with the probe and then chemically functionalizing the end of the nanotube tipped probe with a carboxyl group or amine group so that further chemical modification can be made. This unique chemical functionalization of the nanotube tip can be used to attach a single protein or a specific group of proteins. Such a modified tip can then be used for sensing unique chemical motilities or triggering specific reactions with extraordinary spatial resolution. Functionalized nanotube tips can be used to pattern a substrate for future sensing or chemical logic use.

NANO
LETTERS

2004
Vol. 4, No. 4
725−731

Correlating AFM Probe Morphology to Image Resolution for Single-Wall Carbon Nanotube Tips

Lawrence A. Wade,[†,‡] Ian R. Shapiro,[§] Ziyang Ma,[‡] Stephen R. Quake,[‡] and C. Patrick Collier*[,§]

Jet Propulsion Laboratory and Departments of Applied Physics and Chemistry,
California Institute of Technology, Pasadena, California 91125

Received January 2, 2004; Revised Manuscript Received January 31, 2004

ABSTRACT

Scanning and transmission electron microscopy were used to image hundreds of single-wall carbon nanotube probes and to correlate probe morphology with AFM image resolution. Several methods for fabricating such probes were evaluated, resulting in a procedure that produces image-quality single-wall nanotube probes at a rate compatible with their routine use. Surprisingly, about one-third of the tips image with resolution better than the nanotube probe diameter and, in exceptional cases, with resolution better than 1 nm. This represents the highest lateral resolution reported to date for a SWNT probe.

Single-wall carbon nanotubes (SWNTs) have shown great potential as high-resolution AFM imaging probes.[1−3] The level of resolution possible for both single molecule imaging and force transduction in AFM is ultimately limited by the structure of the tip. Commercially available silicon probe tips have radii of curvature of 5−15 nm. The finest commercially available Si tips are very delicate, leading to substantial variation in tip shape and size even between successive images. SWNTs, on the other hand, have diameters between 1.5 and 6 nm, providing resolution comparable to molecular scale dimensions. Carbon nanotubes are chemically and mechanically robust, with axial Young's moduli of about 1.25 TPa,[4,5] resulting in a tip structure that is stable over prolonged imaging periods.[6] Finally, SWNTs can be chemically functionalized uniquely at their very ends, permitting a broad array of applications in nanotechnology and biotechnology.[7] Nevertheless, it is difficult to reproducibly assemble large quantities of high-quality single-wall nanotube AFM tips. To fully realize the promise of these probes for high-resolution AFM, a better physical understanding is needed of how the geometry of the mounted SWNT on its AFM tip support affects image quality.

Successfully fabricating a probe suitable for AFM imaging in air involves several steps: attaching the nanotube to a silicon AFM tip, shortening it sufficiently to enable high resolution imaging, characterizing its quality, and storing it for later use. Building upon previously reported techniques, we have conducted a comparative survey of fabrication methods to produce a protocol that routinely results in high quality probes. The quality of the AFM images taken with the resultant probes, along with the frequency and ease of success, was used to distinguish between the several approaches studied. In addition, SEM and TEM images of hundreds of nanotube AFM probes were used to evaluate the efficacy of different probe attachment and shortening techniques and to improve the accuracy of our interpretation of AFM imaging and force calibration results. For the first time, the AFM resolution achieved when imaging with nanotube probes was directly correlated to TEM images taken of these same probes. This allowed us to carry out a rigorous examination of nanotube morphology and its influence on image resolution and quality, by directly correlating nanotube geometry, as determined with TEM imaging, with their performance as AFM probes. As a result, we gained significant new insights that are important for research groups performing AFM imaging with SWNT tips.

In this paper, we summarize the results of these studies and describe a procedure that enables consistently successful nanotube probe fabrication. The lateral resolution of these probes when used to image 3 nm diameter SWNTs was typically less than 4 nm, and in one case, 5 Å.[8] This is an improvement by a factor of 4 over the best resolution reported to date using a SWNT probe, which is 2.0 nm.[9] The systematic correlation of TEM images of SWNT probes with the effective lateral resolution obtained when using these probes for topographical imaging indicates that approxi-

---

* Corresponding author. E-mail: collier@caltech.edu.
[†] Jet Propulsion Laboratory.
[‡] Department of Applied Physics.
[§] Department of Chemistry.

10.1021/nl049976q CCC: $27.50

mately one-third of the probes demonstrated resolution smaller than the diameter of the nanotube probe itself when imaging nanotubes on a smooth substrate. For example, we have measured 1.2 nm lateral resolution from a SWNT scanning probe that was 5.5 nm in diameter.

These TEM−AFM correlations provide experimental evidence consistent with previous mechanical modeling carried out by Snow, et al.[10] Additionally, whereas previous investigations have shown nanotube buckling to be an elastic process,[2,3,9,11] we have found that under some circumstances, a SWNT probe can buckle inelastically, resulting in probe damage and corresponding image artifacts.

Finally, we have found that nanotubes picked up by AFM tips can have larger diameters (by about a factor of 2) than the diameters of nanotubes imaged on the surface of the growth substrate, as determined from height measurements with a conventional AFM tip. A better understanding of this discrepancy is needed for optimizing the yield and reproducibility of nanotube probe fabrication. The AFM image resolution statistics we report here underscore the variability between probes fabricated by different methods.

Digital Instruments BioScope and Multimode atomic force microscopes were used with Nanoscope IV controllers for this work. Transmission electron microscopy was performed with a Phillips EM430, and scanning electron microscopy was performed with a Hitachi 4100.

We compared several methods for attaching nanotubes to silicon AFM tips: manual assembly, direct growth, and pickup. Smalley's group reported the first example of the use of carbon nanotubes as AFM tips in 1996.[11] Manual assembly of AFM probes was found to be relatively simple, although the nanotubes had to be large enough to be seen and manipulated under an optical microscope, and thus did not yield high-resolution probes. While direct growth[12−14] offers the potential for parallel fabrication of SWNT AFM probes, we found that the yield was quite low. We also determined that the rate-limiting step in probe fabrication was the nanotube shortening step rather than attachment. Therefore, we focused our efforts on the pick-up technique for nanotube attachment, as shown in Figure 1.

The pick-up technique, developed by Lieber et al.,[15] is an efficient and consistent method for mounting SWNTs in the proper orientation. When SWNTs are grown on a flat substrate, a small percentage of the tubes are oriented vertically, and can be picked up when the AFM tip scans across the surface in tapping mode. The nanotube binds to the side of the pyramidal AFM tip via attractive van der Waals forces, and usually remains attached firmly enough that it can be repeatedly pressed into and scanned across the substrate surface. We found that it was important to reduce the field of view (e.g., from 10 μm to 10 nm) or retract the tip as soon as a nanotube was successfully picked up in order to minimize the probability of picking up additional nanotubes (see Supporting Information). Multiple attached tubes or bundles can lead to AFM image artifacts.

It is also important to note that the ambient humidity appears to affect the efficiency of the pickup method. We found it nearly impossible to pick up nanotubes from a substrate under high humidity conditions. Enclosing the AFM in a glovebag under a flow of dry nitrogen for about 30 min rejuvenated the process. We speculate that an increase in the relative humidity makes it more difficult to pick up nanotubes for two main reasons. First, at higher humidity values, it is harder to overcome capillary forces due to the build up of a surface layer of water on the growth substrate. More force is necessary to pry a prone nanotube off the surface due to increased adhesion. Second, increasing water build up on the tip decreases the attractive interactions of the nanotube to the silicon surface of the AFM tip during pick up. It is known that the van der Waals interactions at the nanotube−AFM tip interface are not strong enough to keep the tube attached to the tip in liquid water.[9] Nanoscopic condensation of water between the AFM tip and the growth substrate at high relative humidity may have an analogous effect on the success rate for picking up a nanotube.

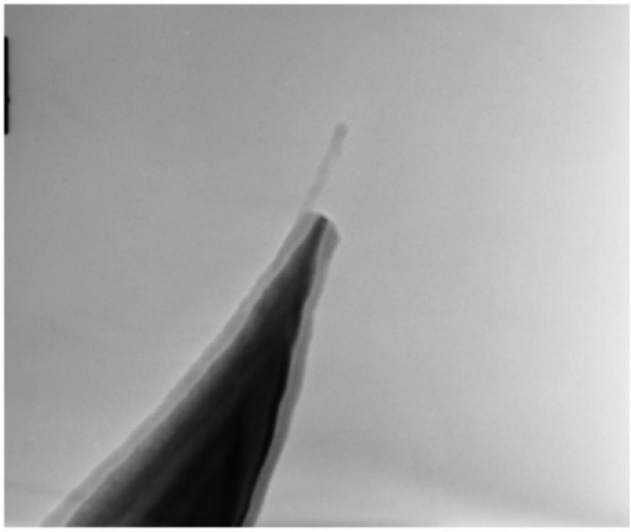

Figure 1. TEM image of a single-wall carbon nanotube picked up from a silicon substrate.

SWNTs were grown via chemical vapor deposition (CVD) on 4 mm to 8 mm square, 500 μm thick p-doped Si wafers. Four different methods were used to coat the substrates with iron catalyst for growing nanotubes suitable for pickup: spin coating a solution of $Fe(NO_3)_3{\cdot}9H_2O$ in isopropyl alcohol,[9] thermal evaporation of iron onto the substrate, electron beam evaporation of iron onto the substrate,[15] and incubation with ferritin. We achieved the most uniform deposition of small (1−2 nm) catalytic sites with high spatial density by using ferritin-derived iron nanoparticles, prepared as described by Dai and co-workers.[16]

CVD growth was performed in a 22 mm inner diameter Lindberg/Blue M quartz tube furnace with a single heating zone 312 mm long, as shown in Figure 2. Five wafers are positioned 12.5 mm apart in a specially designed quartz holder, oriented vertically and with the catalyst-coated side facing away from the direction of the incoming gas. A significant advantage of this holder is that it enables up to three small substrates to be mounted side-by-side in each slot for parallel comparison of growth results under nearly identical temperature and gas flow conditions.

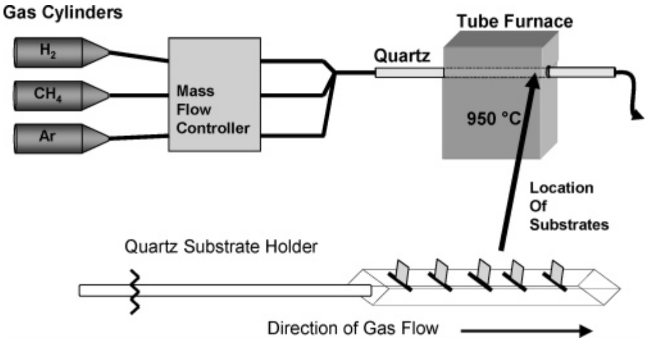

Figure 2. Diagram of CVD apparatus for production of nanotube substrates.

We found that growth was faster (5 μm long nanotubes within one minute) and the distribution of tube lengths increased when the catalyst-coated surface was facing away from the incoming gas flow. We speculate that this is due to increased turbulence of the gas flow at the catalyst coated side after passing over the edges of the substrate. Induced turbulence should minimize the role of diffusion-limited growth relative to nucleation rate in the growth kinetics, but at the expense of uniform growth. These growth procedures generate SWNTs on the substrate with diameters ranging from 1.6 to 3.0 nm, and lengths between 100 nm and 5 μm, as imaged with AFM and SEM.

The distribution of tube diameters varied with the size of the catalytic sites. For example, we found that spin coating many drops of dilute solution of the iron nitrate catalyst to give a high density of small catalytic sites gave a slightly broader tube diameter distribution than did ferritin. In contrast, depositing a few drops of higher density iron solutions yielded broad size distributions and larger average tube diameters. Based on AFM analyses of these substrates, it appears that the larger tube diameters resulted from larger catalytic sites on the substrate. No MWNTs have been observed on these substrates.

The long-term stability of pickup substrates appears to vary depending on how they were prepared. Ferritin and ferric nitrate substrates appear to be substantially less effective for pickup attachment after 4 to 6 months. We hypothesize that this is due to the relatively weak mechanical attachment of the catalytic site to the substrate. Over time, vertically oriented tubes that are attached to loosely bound catalytic sites apparently physisorb onto the substrate. Enclosing the AFM in a glovebag with a flow of dry nitrogen for about 30 min substantially enhanced pickup with these older substrates. In contrast, substrates that had the catalytic sites deposited by molecular beam epitaxy (MBE) have demonstrated reliable pickup of nanotubes with an AFM tip over several years without special care.[15]

The diameters of the picked up tubes measured with TEM were typically between 4 and 6 nm. In comparison, the diameters of nanotubes lying horizontally on the substrate, determined by AFM height measurements, were only 2−3 nm. We have ruled out TEM and AFM calibration errors as the cause of this discrepancy. We have also ruled out compression of the imaged nanotubes by the AFM tip, which would result in a decreased apparent diameter. Deformation of the horizontal nanotubes due to van der Waals forces has also been modeled using realistic molecular dynamics simulations based on quantum mechanical calculations, and found insufficient to explain this discrepancy.[17] It appears that this disparity is real and not just an artifact due to tube distortion or measurement error.

This indicates a strong preference for larger diameter tubes to be picked up by silicon AFM probes. There are two plausible explanations for this disparity. One possibility is that larger diameter nanotubes have a higher probability of remaining vertically oriented on the growth substrate over time than smaller diameter tubes. Only the population of smaller diameter nanotubes adsorbed to the growth substrate can be imaged by AFM. Hence, AFM images will be biased toward this part of the distribution of nanotube diameters.

Alternatively, this disparity may be explained by the binding energy of the nanotube to the AFM cantilever tip relative to the binding energy of the nanotube to the substrate. Once a SWNT has been picked up by a scanning AFM tip, there are two kinds of motions that impose stress on the system. The AFM cantilever has a net motion parallel to the substrate. During pick-up, typical horizontal velocities are on the order of 30 000 nm/s. This motion imposes three kinds of stress on the system: shear, bending, and tension. In addition, the cantilever has a rapid vertical oscillation, typically 70−250 kHz, with an amplitude of 40−50 nm, that imposes additional bending and tension stresses.

The mechanical stresses imposed by the cantilever motion on a nanotube attached on one end to the AFM tip, and on the other end to the surface of the growth substrate, will result in one of two outcomes: the nanotube either slips off the cantilever tip and remains attached to the substrate, or the nanotube separates from the substrate interface and is "picked up". The discriminator between these two outcomes is the binding energy at the attachment site of the nanotube to the silicon tip relative to that of its attachment to the substrate. These binding energies will depend on many factors that are virtually impossible to characterize fully, such as the relative lengths of the nanotube adsorbed onto the tip versus the substrate, as well as details of the chemical, physical, and mechanical interactions between the nanotube and these surfaces during scanning in tapping mode. It is known, however, that binding energy scales with the tube diameter, which can be determined directly from both AFM and TEM images.

The strength of nanotube attachment can be approximated as being linearly proportional to the nanotube diameter using the thin-walled cylinder approximation. At the attachment site with the AFM cantilever tip, the nanotube can be considered fixed until the binding energy is exceeded at this interface by the imposed stresses. This binding force increases linearly with diameter, but at a rate 1.6 times faster for tubes greater than 2.7 nm diameter than it does for smaller diameter nanotubes.[18] The increased binding energy for nanotubes greater than 2.7 nm could result in larger diameter nanotubes being preferentially picked up. The relative adhesion strength of the catalytic particle to the tube versus the substrate could also have a significant influence on the diameters of the tubes that are picked up.

As seen in Figure 1, more than 100 nm of a nanotube typically protrudes from the end of the AFM tip after pick-up. High-resolution imaging is not possible with such a long nanotube tip due to thermal fluctuations and bending. Pick-up SWNT tips were shortened by a combination of push shortening, an approach developed by Hafner and Lieber,[13] and electrical pulse etching.[2,12] An HP 8114A pulse generator was used in combination with a Digital Instruments signal access module for all of our pulse shortening experiments.

Push shortening is done by incrementally decreasing the tip−sample separation distance during successive force calibrations to push the nanotube up along the side of an AFM tip. This process requires a picked-up tube of very specific length. Tubes longer than 100 nm tend to buckle inelastically during this process, after which they cannot be shortened by further pushing. Push shortening is superior to pulse etching when further shortening nanotubes less than 100 nm long in very small increments.

We obtain similar results for electrical pulse etching with native oxide coated p-doped silicon, 300 nm thick thermally grown oxide-coated p-doped silicon, and gold-plated silicon substrates. This finding indicates that the entire probe fabrication procedure can be carried out on a single unpatterned, doped-silicon substrate. Thermally grown oxide substrates typically required higher voltages to successfully pulse-shorten than did either native oxide or gold-coated silicon substrates.

Using electrical pulse shortening and push shortening in combination on the same tip relaxes the constraints for obtaining high-quality probes from the nanotube growth substrate and increases yield. Long tubes can be coarsely shortened with electrical pulses until their lengths are less than 100 nm. Push shortening can then be used for finer control in adjusting the probe length.

We frequently found that electrostatic forces would strip nanotubes off the AFM tips when they had been stored in a nonconductive container. An aluminum box with a narrow strip of double-sided tape or a conductive Gel-Pak container both seemed to solve this problem. Prior to use of conductive boxes for nanotube tip storage, we were unsuccessful in TEM imaging the attached nanotube probes.

To characterize the effective resolution of our SWNT probes, we imaged nanotubes resting flat on the silicon growth substrate, using a scanning field of view of 100−350 nm. We define resolution as the full width of the imaged tube measured at the noise floor, minus the measured tube height. While nanotubes are convenient samples for determining resolution, they are not infinitely rigid. Dekker's group has shown that the apparent height of a nanotube measured by tapping mode imaging can decrease substantially at high oscillation amplitudes, even with conventional silicon tips.[19] We have observed similar effects with nanotube probes.[20] For this study, the oscillation amplitude was maintained close enough to its freely oscillating value in air to limit this effect to be within 10% of the true nanotube height.

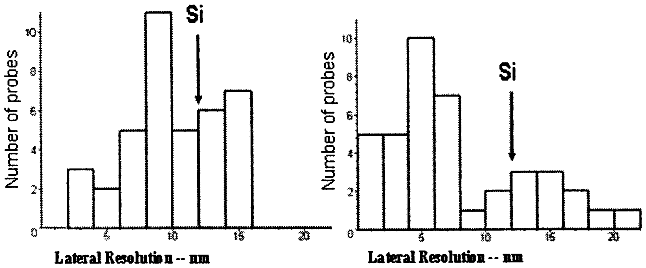

Figure 3. The left histogram summarizes the resolution for 39 probes fabricated on a substrate coated with ferric nitrate catalyst. The right histogram shows the resolution distribution of 40 probes made from nanotubes picked up from a substrate coated with ferritin. Included is the typical resolution obtainable with a conventional silicon AFM tip.

Figure 3 shows histograms of the lateral resolutions obtained with SWNT probes fabricated using a growth substrate coated with ferric nitrate catalyst versus those fabricated using ferritin as the catalyst. The variation in nanotube probe performance was greater than we expected based on previous reports. Leiber et al. had examined the image quality of different nanotube types (MWNTs and SWNTs).[21] In contrast, we compared 39 SWNTs made from the same iron nitrate-coated substrate and 40 from a ferritin substrate. The wide range in resolution found, between the two different kinds of substrate (ferritin vs iron nitrate), as well as from the same substrate, was surprising and underscores the importance of specific nanotube characteristics in determining the maximum achievable resolution.

There is a clear shift in the distribution toward higher resolution probes when ferritin was used as the catalyst, consistent with a narrower catalyst size distribution. It is not clear how much technique improvements rather than the switch to ferritin from ferric nitrate coated substrates played in the comparative distribution. Most of the latter tips were fabricated using ferritin substrates. By that time, we were more careful to reduce the field of view immediately after pick-up to minimize bundle formation. This could explain why there are fewer 10−15 nm resolution tips. However, it is clear that significantly more probes with resolution better than 5 nm were fabricated using ferritin substrates.

Nearly 100 probes were imaged by TEM to characterize the efficacy of different fabrication techniques. Of these, fourteen SWNT probes imaged by TEM had previously been used for tapping-mode topographic imaging. Table 1 presents a summary of probe characteristics determined by TEM−AFM correlations for the fourteen SWNT probes. Entries in bold correspond to probes that demonstrated lateral resolution less than the actual nanotube probe diameter.

Image quality is a function of many factors including: tube diameter and length, contact angle, number of nanotubes extending past the silicon tip, thermal noise, and contamination. These factors can lead to substantial variability in resolution. By correlating probe structure and orientation seen in the TEM images with topographic imaging performance, we can provide experimental evidence consistent with previous mechanical modeling carried out by Snow et al.,[10] who have shown that lateral tip−sample forces can bend

Table 1. TEM−AFM Correlation Table for Single-Wall Carbon Nanotube Scanning Probes

tip type	tube diameter	tube length	aspect ratio	deviation from perpendicular	lateral resolution (full width-height)	lateral resolution/ probe diameter
SWNT	**4.2 nm**	**10 nm**	**2.4**	**10°**	**2.8 nm**	**0.67**
Bundle	**9.3 nm**	**77 nm**	**8.3**	**20°**	**4.0 nm**	**0.43**
SWNT	4.0 nm	112 nm	28	30°	10.4 nm	2.60
SWNT[a]	4.0 nm	19 nm	4.8	40°	4.6 nm	1.15
SWNT	**5.5 nm**	**40 nm**	**7.3**	**20°**	**1.2 nm**	**0.22**
Bundle	**8.0 nm**	**35 nm**	**4.4**	**15°**	**5.6 nm**	**0.70**
SWNT	3.7 nm	30 nm	8.1	30°	5.8 nm	1.56
SWNT[a,b]	4.2 nm	33 nm	7.9	20°	6.0 nm	1.43
SWNT	5.4 nm	38 nm	7.0	10°	5.9 nm	1.09
SWNT	3.5 nm	15 nm	4.3	20°	4.4 nm	1.26
Bundle	5.5 nm	51 nm	9.3	0°	21 nm	4.0
SWNT	**5.3 nm**	**55 nm**	**10.4**	**0°**	**3.9 nm**	**0.74**
SWNT	**6.5 nm**	**42 nm**	**6.5**	**0°**	**4.3 nm**	**0.66**
SWNT	5.4 nm	26 nm	4.8	10°	8.0 nm	1.48

[a] Probe showed a “shadowing” artifact. [b] Nanotube appeared buckled 16 nm from the end of the tube.

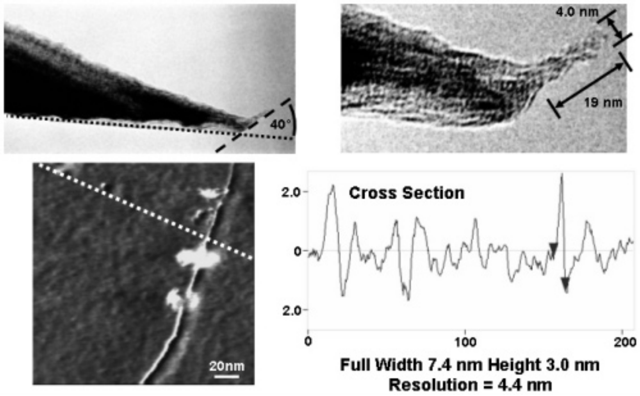

Figure 4. Correlation of image showing artifact due to large contact angle with substrate. Additionally, this nanotube appears to be buckled near the silicon tip. The dotted black line in the upper left image is perpendicular to the substrate.

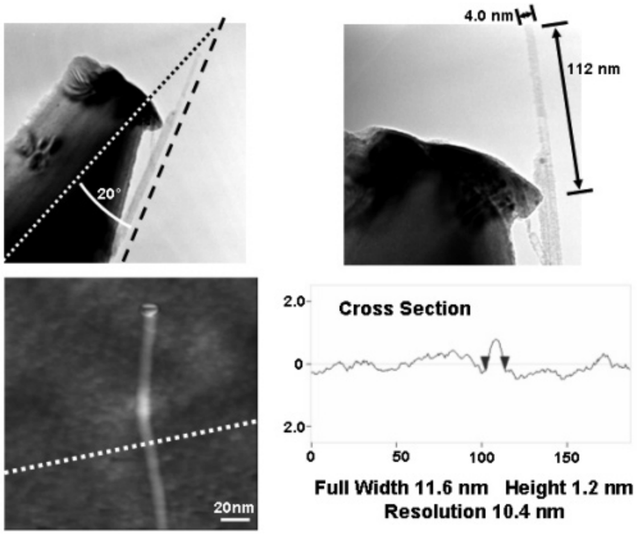

Figure 5. Image artifacts due to bending are significant for long nanotubes. Note that there are a number of picked up nanotubes at the base of this tip. The damage to the silicon tip probably occurred during repeated force calibrations.

single-wall nanotubes or cause snap-to-contact behavior when the tubes exceed either a critical length or a critical angle relative to the substrate surface normal. These effects introduce a significant degree of broadening and the appearance of image artifacts.

If the nanotube is presented to the sample surface at an angle deviating from the surface normal by more than ∼30°, poor resolution and obvious image artifacts result due to tip−sample forces having a significant component perpendicular to the nanotube axis. For example, Figure 4 shows a 19 nm long, 4 nm diameter nanotube projecting from the probe tip at an angle of 40°. This probe produced an image that contained a positive height “shadowing” artifact approximately 10 nm in width parallel to each sample nanotube. This artifact resulted from the nonideal orientation of the probe. Additionally, the TEM image showed that the nanotube is buckled near the silicon tip. Previous reports have described reversible *elastic* buckling of the nanotube, which did not have a serious impact on image quality.[5,9,21] Our TEM correlations indicate, however, that buckling can, under some circumstances, be inelastic, resulting in irreversible structural changes. This structural defect results in an effectively lower stiffness for the probe, which we believe is responsible for the decreased resolution and imaging artifacts we observe (shadowing features). Similar artifacts were seen with SWNT ropes (multiple SWNTs bundled together) for the same reason; the layered structure of a bundle of nanotubes attached to the AFM tip results in stiffness variation along the probe length.

SWNTs must also have aspect ratios less than ∼10 to be adequate for imaging purposes. Figure 5 shows a 4 nm diameter nanotube protruding 112 nm from the end of the AFM tip, but at an angle deviating from the surface normal by less than 20°. The resulting lateral resolution was still 2.5 times the probe tube diameter. This broadening of the image is due in small part to thermal vibrations. However, mechanical modeling studies have indicated that for a nanotube of this geometry, the root-mean-squared thermal vibrations of the end of the tube should be less than 2 Å.[22] Nanotube bending due to lateral tip−sample forces is most likely the principal contribution to the degraded resolution.

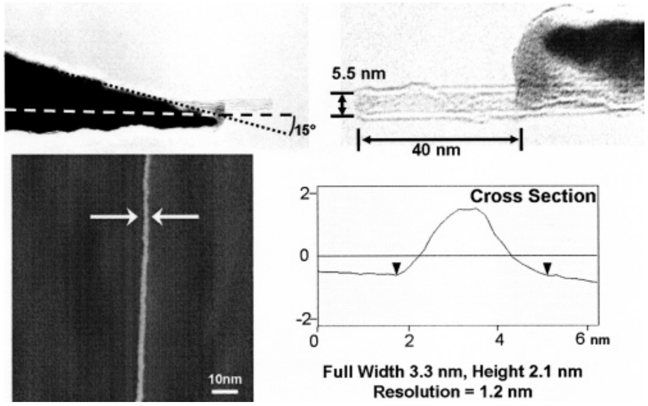

Figure 6. TEM−AFM correlation of a SWNT probe that demonstrated an effective lateral resolution that was 22% of the probe diameter.

Images taken with high quality nanotube probes show no sign of artifacts. These probes all had the nanotubes oriented on the tip at angles close to the substrate surface normal (within 10−20°) and had protrusion lengths $\leq$40 nm. By directly measuring the nanotube width from each TEM image and comparing that to the obtained AFM resolution, we have determined the average ratio of AFM resolution to tube diameter for SWNT probes in this class to be 1.17. This is a reasonable value, given that thermal vibrations and bending of the nanotube will always slightly increase its effective imaging diameter.

In about 1/3 of the high quality nanotube probes made from the ferritin substrate, as shown in Figure 6, it was found that the effective lateral resolution was significantly *better* than the nanotube probe diameter measured directly with TEM. Figure 6 shows a nanotube probe 5.5 nm in diameter that demonstrated a lateral resolution of 1.2 nm, just 22% of the diameter of the nanotube. It is likely that this enhanced resolution occurs when the nanotube contacts the substrate being imaged with either an asperity or at a specific angle such that only an edge of the nanotube is in contact with the substrate. Imaging a small object with an asperity or an open edge of the tube could lead to the high resolutions observed. Molecular dynamics simulations of surface−nanotube and nanotube−nanotube interactions indicate that other phenomena may also be important, including elastic deformation of the sample nanotube relative to the probe nanotube.[17]

In conclusion, we have combined elements from several previously reported techniques for producing nanotube tips suitable for AFM imaging dry samples that significantly reduce the time of manufacture while improving reproducibility and performance. Feedback from SEM and TEM images of the nanotube probes was used to directly evaluate the effectiveness of the different techniques employed for each of the steps in the fabrication procedure. The optimal process involves the following six steps. (1) Grow nanotubes from ferritin-derived iron nanoparticles on conductive silicon substrates coated only with its native oxide. (2) Pick up a SWNT by imaging the substrate with a 10 μm field of view in tapping mode. (3) Quickly reduce the field of view to approximately 10 nm so that additional tubes are not picked up. (4) Shorten the tube to an appropriate length for imaging without changing substrates using a combination of electrical pulse and push shortening techniques. (5) Image a 100−500 nm region of the substrate to characterize the probe quality. (6) Store shortened nanotube probe in a conductive box.

By growing nanotubes directly on a conductive p-doped silicon substrate with only a native oxide layer, it is possible to pick up, shorten, and test the probe resolution without having to switch samples. This proved to be a significant timesaving optimization. We have found that the resulting nanotube growths (diameter and length) are very similar for all of the investigated catalyst deposition techniques if the spatial density and diameters of catalytic sites are similar. Rates of production have typically reached one probe per hour for several consecutive hours. On exceptional days, the rate can be as high as several per hour. This success has been duplicated with incoming group members.

Overall, we have found AFM image quality to be consistently and significantly better with nanotube tips than with the best silicon AFM tips. Correlations of TEM images of SWNT probes with the effective lateral resolution obtained when using these probes for topographical imaging with AFM indicate that approximately one-third of the probes demonstrate resolution better than the diameter of the nanotube probe itself when imaging nanotubes on a smooth substrate. The methodology described here has resulted in a sufficiently high level of productivity to enable development of single-molecule probes and sensors using functionalized nanotube tips, and has proven capable of fabricating AFM probes with the highest resolution reported to date.

Acknowledgment. The authors thank Jason Hafner, Jim Hone, and Jordan Gerton for fruitful discussions and suggestions. We also thank Carol Garland for many patient hours of TEM imaging and NanoDevices, Santa Barbara, CA for providing direct growth nanotube tips for characterization. Wade, Ma, and Quake were supported by a grant from Pharmagenomix; Shapiro and Collier were supported by Caltech startup funds. Wade, Shapiro, and Collier were also supported by the Caltech President's Fund and NASA contract NAS7-1407.

Supporting Information Available: Experimental procedures for SWNT growth and AFM probe fabrication. This material is available free of charge via the Internet at http://pubs.acs.org.

References

(1) Hafner, J. H.; Cheung, C.-L.; Wooley, A. T.; Lieber, C. M. *Prog. Biophys. Mol. Biol.* **2001**, *77*, 73.
(2) Wong, S. S.; Harper, J. D.; Lansbury; P. T., Jr.; Lieber, C. M. *J. Am. Chem. Soc.* **1998**, *120*, 603.
(3) Wong, S. S.; Woolley, A. T.; Odom, T. W.; Huang, J. L.; Kim, P.; Vezenov, D. V.; Lieber, C. M. *Appl. Phys. Lett.* **1998**, *73*, 3465.
(4) Krishnan, A.; Dujardin, E.; Ebbesen, T. W.; Yianilos, P. N.; Treacy, M. M. J. *Phys. Rev. B* **1988**, *58*, 14013.
(5) Wong, E. W.; Sheehan, P. E.; Lieber, C. M. *Science* **1997**, *277*, 1971.
(6) Larsen, T.; Moloni, K.; Flack, F.; Eriksson, M. A.; Lagally, M. G.; Black, C. T. *Appl. Phys. Lett.* **2002**, *80*, 1996.
(7) Wong, S. S.; Joselevich, E.; Wooley, A. T.; Cheung C.-L.; Lieber, C. M. *Nature* **1998**, *394*, 52.

(8) Wade, L. A.; Shapiro, I. R.; Ziyang, M.; Quake, S. R.; Collier, C. P. *Nanotech 2003* **2003**, *3*, 317.

(9) Hafner, J. H.; Cheung, C.-L.; Oosterkamp, T. H.; Lieber, C. M. *J. Phys. Chem. B* **2001**, *105*, 743.

(10) Snow, E. S.; Campbell, P. M.; Novak, J. P. *Appl. Phys. Lett.* **2002**, *80*, 2002.

(11) Dai, H.; Hafner, J. H.; Rinzler, A. G.; Colbert, D. T.; Smalley, R. E. *Nature* **1996**, *384*, 147.

(12) Cooper, E. B.; Manalis, S. R.; Fang, H.; Dai, H.; Minne, S. C.; Hunt, T.; Quate, C. F. *Appl. Phys. Lett*. **1999**, *75*, 3566.

(13) Hafner, J. H.; Cheung, C. L.; Lieber, C. M. *J. Am. Chem. Soc.* **1999**, *121*, 9750.

(14) Hafner, J. H.; Cheung, C.-L.; Lieber, C. M. *Nature* **1999**, *398*, 761.

(15) Hafner, J.; Rice University, private communication, March, 2002.

(16) Li, Y.; Kim, J. W.; Zhang, Y.; Rolandi, M.; Wang, D.; Dai, H. *J. Phys. Chem. B* **2001**, *105*, 11424.

(17) Shapiro, I. R.; Solares, S.; Esplandiu, M. J.; Wade, L. A.; Quake, S. R.; Goddard, W. A.; Collier, C. P., manuscript in preparation.

(18) Hertel, T.; Walkup, R. E.; Avouris, Ph. *Phys. Rev. B* **1998**, *58*, 13870.

(19) Postma, H. W. C.; Sellmeijer, A.; Dekker, C. *Adv. Mater.* **2000**, *12*, 1299.

(20) Esplandiu, M. J.; Shapiro, I. R.; Solares, S.; Matsuda, Y.; Goddard, W. A.; Collier, C. P., manuscript in preparation.

(21) Cheung, C. L.; Hafner J. H.; Lieber, C.; M. *Proc. Natl. Acad. Sci. U.S.A.* **2000**, *97*, 3809.

(22) Yakobson, B. I.; Avouris, Ph. *Topics Appl. Phys.* **2001**, *80*, 287.

NL049976Q

Supplemental information for NanoLetters, 2004, Vol. 4, 725-731.

Correlating AFM Probe Morphology to Image Resolution for Single Wall Carbon Nanotube Tips

*Lawrence A. Wade,[1,2] Ian R. Shapiro,[3] Ziyang Ma,[2] Stephen R. Quake,[2] C. Patrick Collier[3]**

[1]Jet Propulsion Laboratory, [2]Department of Applied Physics, [3]Department of Chemistry

California Institute of Technology, Pasadena, CA 91125

collier@caltech.edu

Supporting Information:

Nanotube AFM Tip Attachment

Methods we compared for attaching nanotubes to silicon AFM tips include manual assembly, direct growth and pickup.

Smalley's group reported the first example of the use of carbon nanotubes as AFM tips in 1996.[1] They manually attached multi-wall carbon nanotubes (MWNT) and ropes of individual SWNTs to the apex of silicon pyramidal tips using tape adhesive and a micromanipulator in an optical microscope. The main drawback to this method is that MWNT tips large enough to be seen optically did not improve the resolution much beyond standard silicon tips when imaging isolated amyloid fibrils.[2]

We found it fairly efficient to manually attach MWNTs to silicon AFM cantilevers with a 1000x optical microscope. In particular, the rate of assembly was quite high when a 15 V potential was applied between the silicon probe and the nanotubes. This resulted in nearly perfect and rapid alignment of the nanotube to the silicon tip. However, there was not a clear path to doing so with the thin SWNTs required for very high-resolution imaging.

Lieber[3,4] and Quate's[5] groups later showed that individual single wall carbon nanotubes could be directly grown by chemical vapor deposition (CVD) on the silicon tips themselves by first pre-coating the tip with a metal catalyst. In the CVD synthesis of carbon nanotubes, metal catalyst nanoparticles are heated in the presence of a hydrocarbon gas or carbon monoxide; the gas molecules dissociate on the catalyst surface and carbon is adsorbed into the particle. As the carbon precipitates, a carbon nanotube is grown with a diameter similar to that of the catalyst particle.

Two techniques for direct growth have been reported. One involves creating nanopores at the apex of the silicon tip by etching with hydrofluoric acid. Catalyst particles are then deposited inside the nanopores. Carbon nanotubes grown via CVD from such a tip have an appropriate geometry for AFM imaging. While this approach enables fabrication of SWNT tips, the preparation of the porous layer in the silicon is time consuming and placement of the nanotube at the optimal location near the tip apex is often not achieved. In addition nanotubes typically grew at perhaps 1% of catalytic sites for the growth procedures we have explored. To ensure a moderate probability of having a nanotube grown on a given tip, a large number (20 or more) of etched holes with catalytic particles could be fabricated. However, any given tip might have no tubes, one tube or several tubes.

Direct surface growth of SWNTs by CVD on catalyst-coated silicon tips has also been demonstrated, without the use of pores. We have analyzed approximately 300 tips prepared this way with scanning electron microscopy (SEM) and dozens of tips with transmission electron microscopy (TEM). As seen in Figure 1, we most commonly found densely coated tips with ropes and bundles of SWNTs extending from all sides of the silicon pyramid. These ropes often form complex loop structures not suitable for AFM work. About 1/3 of the tips examined had no tubes near the tip although they may have been covered by nanotubes elsewhere. Only a few percent of the probes had single nanotubes at the tip. Even fewer were oriented vertically.

The mechanical stability of the nanotubes directly grown on the silicon tips was found to be quite poor. As a control, we briefly imaged a smooth surface in tapping mode with tips having nanotubes at the end, as determined by SEM, before any attempts at electrical pulse shortening of the tubes. Afterwards, these probes were re-imaged by SEM. The nanotubes were lost from 7 of 9 tips used in this control experiment. It was also frequently observed during electrical pulse shortening that the tubes would fall off. The final yield of useful nanotube tips was therefore on the order of 1% of the number of originally fabricated probes using the direct growth method. While these results represent early attempts at developing nanotube AFM tips, and there was clearly significant progress possible with continued process development, we decided to focus on the technically simpler problem of developing suitable substrates for nanotube pickup.

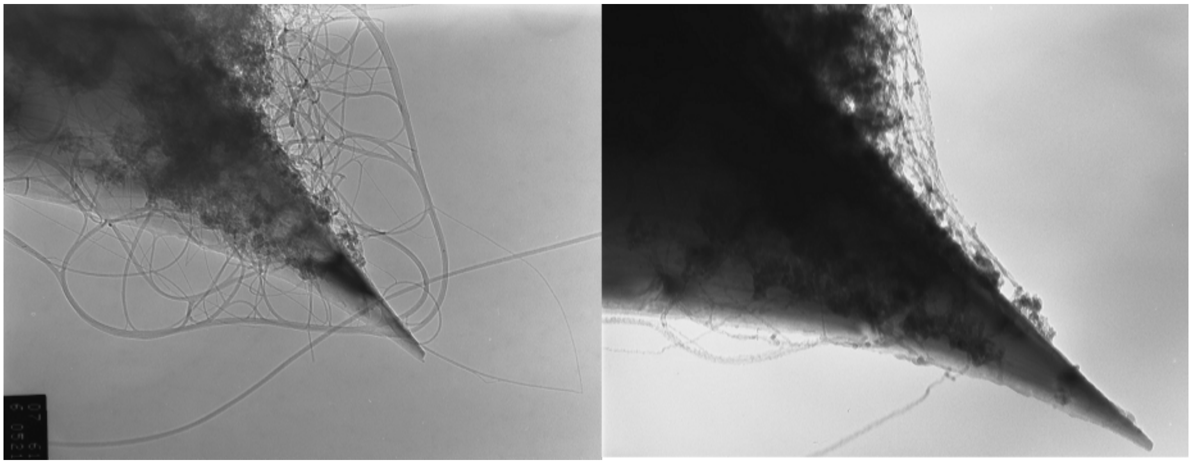

Figure 1. TEM images of nanotubes grown on AFM tip include ropes, multi-walled and single-walled tubes. Note that most of the growths consist of ropes.

Pick-up Substrate Preparation and Nanotube Growth

The pick-up technique is an efficient and consistent method for mounting SWNTs in the proper orientation. When SWNTs are grown on a flat substrate, a small percentage of the tubes are oriented vertically, and can be picked up when the AFM tip scans across the surface in tapping mode. Typically, 1 to 4 tubes can be picked up from a 10 μm square region. Given this tube density, a 6 mm substrate could in theory be used nearly a million times. Nanotube substrates suitable for pickup were produced using four methods of catalyst deposition and compared in side-by-side CVD growths. We achieved similar results with each of these techniques. The suitability of a substrate for nanotube pickup appears to depend primarily on the density and size distribution of the catalytic sites and not on how they were deposited.

Pick-up of a nanotube is readily observed by monitoring the height signal of the AFM image while looking for a significant step change in the average position. The nanotube binds to the side of the pyramidal AFM tip via attractive van der Waals forces, and usually remains attached firmly enough that it can be repeatedly pressed into and scanned across the substrate surface. A picked up tube can be removed by holding the tip a few hundred nanometers above the substrate and applying a 50V, 100 µs pulse. The removal mechanism is not clear but probably involves either electrostatic attraction or ablation.

Nanotube pick up can reoccur several times, resulting in a 'bundle' of nanotubes attached to the tip. In figure 2, two bundles are shown that most likely were picked up sequentially, although it is possible that they grew this way on the substrate.

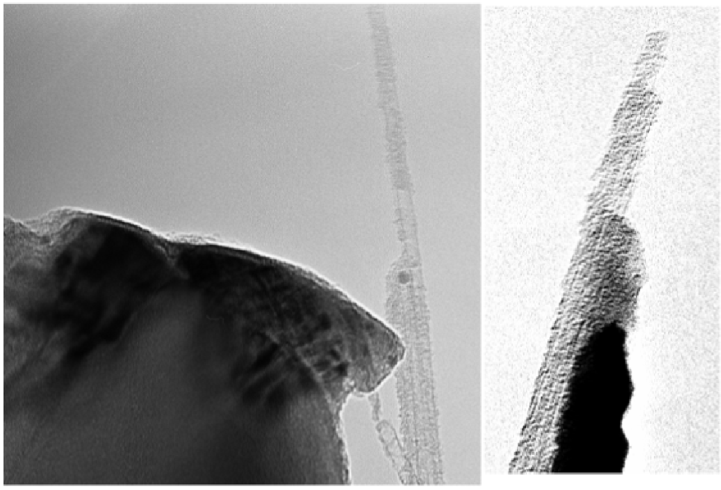

Figure 2. Several tubes have been picked up and stacked in 'bundles' on silicon AFM probes.

Silicon substrates were cleaved under cleanroom conditions, and cleaned by sonicating for 15 minutes at 25 ºC first in toluene, then in acetone, and finally in electronics-grade isopropyl alcohol. To coat the substrates with catalytic iron nanoparticles, 1-30 drops of 1-30 µg/mL $Fe(NO_3)_3$•$9H_2O$ solution in electronics-grade isopropyl alcohol were applied while spinning substrates at 3000 r.p.m., waiting approximately 10 seconds between drops to permit the solvent to evaporate. We found that the catalytic sites would be considerably larger and often less homogeneously distributed over the surface at higher concentrations (e.g. 100-300 µg/mL $Fe(NO_3)_3$•$9H_2O$). The nanotube growths on such substrates were correspondingly larger in diameter and sparser. Again, the critical factor is achieving a high density of very small catalytic sites.

Alternately, some silicon substrates were coated under high vacuum with ~1/40 monolayer of iron applied by thermal or electron beam evaporation. In general, the deposited catalyst sites were large and not optimal for SWNT growth. However, with continued development an optimal pickup substrate could most likely be fabricated via molecular beam epitaxy of the iron catalyst at patterned growth sites. Such a substrate can achieve a nearly uniform catalyst site size and therefore will grow a more uniform distribution of nanotubes; a high density of 1-3 nm diameter tubes with lengths less than 1 µm would be ideal. In addition, such a substrate is substantially more stable over time and can be used for nanotube pickup successfully for several years.

Other silicon substrates were incubated overnight at 4 ºC in a 44 µM solution of ferritin containing ~200 Fe atoms/protein, prepared as described by Dai and coworkers.[6] In this process, a calcination step is required after coating the substrate to remove all organic material originating from the ferritin protein, leaving behind only nanoparticles of iron oxide. This is done by heating the coated substrate in a furnace to 800 ºC in air and holding at that temperature for 10 minutes. This process gave the smallest catalyst size distribution and therefore yielded the most consistent nanotube growths. The catalytic site size distribution and the resultant growths were very consistent with those reported by Dai. The results from a typical ferritin growth are depicted in Figure 3.

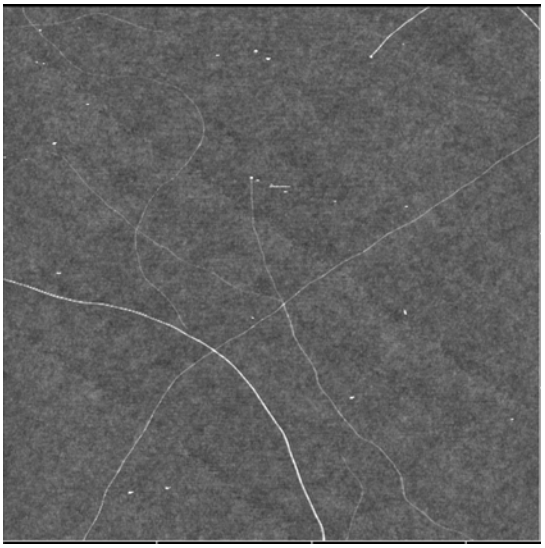

Figure 3. AFM height image of nanotubes grown from ferritin coated oxidized silicon substrate. Field of view is 3 x 3 μm. The height range is 10 nm.

CVD growth was performed in a 22 mm inner diameter Lindberg/Blue M quartz tube furnace with a single heating zone 312 mm long. Five wafers are positioned 12.5 mm apart in a specially designed quartz holder, oriented vertically and with the catalyst coated side facing away from the direction of the incoming gas. A significant advantage of this holder is that it enables up to three small substrates to be mounted side-by-side in each slot for parallel comparison of growth results under nearly identical temperature and gas flow conditions. Optimal nanotube growth is obtained when the holder is positioned at the leeward end of the quartz tube, with the last wafer approximately 2 mm from the end of the heating zone.

The quartz tube is then flushed for 15 minutes with argon gas (Matheson, 99.9995% purity, 440 sccm). The furnace is heated at 950˚ C for approximately 20 minutes, and then held at 950˚C for 15 minutes, both under a flowing atmosphere of Argon (440 sccm) and H_2 (Matheson, research grade, 125 sccm). The furnace is held at this temperature for 5 additional minutes while being flushed with Ar (440 sccm). Growth of nanotubes is then carried out for 0.5 to 2 minutes at 950˚C with CH_4 (Air Liquide, Ultra High Purity, 1080 sccm) and H_2 (125 sccm). Following this growth step, the furnace is again flushed with Argon (440 sccm) and held at 950˚C before rapidly cooling to less than 250˚C, after which the substrates are removed from the furnace.

Substantial variations in growth density occurred between substrates mounted at different positions in the furnace or between identically placed substrates on different runs, which we attribute to temperature variations in the furnace. It was found that the substrate temperature could differ by as much as 20 ˚C with a 1 cm change in position in the furnace or upon changes in the gas composition and mass-flow. A three-stage furnace would likely help improve reproducibility.

Shortening AFM Nanotube Tips

Push and electrical pulse techniques for shortening nanotube AFM tips were examined individually and in combination. This was done on several different surfaces. The most efficient method was to combine pickup, pulse and push shortening all on a single substrate. Force calibration measurements were employed to establish the length of the nanotube tips using the method described by Cooper, *et al.*[5] This approach was found to be suitable for both push and electrical pulse shortening techniques. Once a nanotube has been picked up and shortened, the probe can be used for high-resolution imaging, biomolecular manipulations or force spectroscopy.

A general method for shortening utilizes electrical pulses.[2,7] The procedure to shorten the SWNT in air consists of applying +5 to +30 volt pulses of 20 to 100 μs duration between the AFM tip and a grounded, conductive substrate. Presumably the electrical pulse shortens the nanotube by ablation due to the very high electric field generated at the nanotube end. These pulses are supplied from a Hewlett-Packard 8114A pulse generator and routed to the tip through a Digital Instruments Signal Access Module, or “break-out” box, which is connected to the MultiMode AFM. The pulses are applied while tapping the surface at approximately 70 kHz or 300 kHz, which are the resonance frequencies of the cantilevers we used (FESP and TESP cantilevers, Digital Instruments). While both work, we tend to prefer the softer FESP probes.

For a given SWNT tip, larger voltage pulses shorten the tube in larger increments, as do pulses of longer duration. But the voltage necessary to carry out shortening varies drastically between individual tubes. This is believed due both to the environmental conditions (especially humidity), and to the widely varying conductivities associated with nanotubes of slightly different molecular structure, for example, between semiconducting and metallic nanotubes. Nanotubes can be shortened precisely with steps as small as 2 nm per pulse. The main drawback to this technique is that the nanotube length removed can vary significantly from one pulse to another and one day to another. Hence to successfully employ this technique one must be careful and attentive. A secondary drawback is that electrical pulsing can dislodge the nanotube electrostatically from the AFM tip. Nevertheless, this second effect can also be exploited to controllably deposit nanotubes precisely on substrates for device fabrication.[8]

Push shortening of short, <100nm long tubes is accomplished by taking successive tip-substrate distance-sweep measurements, and incrementing the sweep start point by ~5 nm at a time.[9] By doing this, the tube can be pushed up along the tip. We find electrical pulse shortening to be more effective than push shortening in terms of being able to shorten a nanotube significantly (e.g. by several hundred nm in 20 nm steps).

For substrates with tubes of significantly varying length that are typically too long the combined approach, pulse shortening followed by push shortening has significant advantages. We have avoided the need for multiple substrates or a patterned substrate that includes pickup and separate shortening regions by reducing the field-of-view to ~10 nm during shortening.

Once the nanotube probe has been shortened to a useful length, the field of view can be increased to 100-500 nm so that a nanotube laying flat on the substrate can be imaged. An AFM image of a horizontal nanotube is a very good way to determine the quality of the final probe. Keeping the field of view small minimizes the chance that another nanotube is picked up.

Imaging with Nanotube Probe Tips

Table 1 in the manuscript lists the properties of 14 nanotube probes that were determined by TEM-AFM correlations described in the text. We have found that topographic image resolution when using SWNT probes was more sensitive to imaging conditions, particularly oscillation amplitude, than conventional silicon probes. This may be due to the small interaction area and compressibility of SWNTs. In addition, in about a third of the cases, the observed AFM resolution was significantly better than would be predicted from the nanotube probe diameter. We have also found that, at a given oscillation amplitude, a small change in drive frequency or in amplitude setpoint can improve image resolution when compared with the optimal settings used for imaging with a bare silicon probe. In particular, the amplitude set point for a nanotube probe can often be as high as 95% of the free oscillation amplitude in air and still permit high resolution imaging. A high amplitude setpoint corresponds to small tip-sample forces, which is desirable for imaging delicate biological macromolecules.

When imaging with SWNT tips in tapping mode AFM, care must be taken to recognize imaging artifacts. Imaging artifacts can be introduced through bending and thermal vibration.[10] In addition, buckled nanotubes frequently demonstrate degraded resolution or artifacts. We have also seen multiple tubes at the tip of some probes, either bundled together to form a "broom", or attached to different faces of the silicon AFM tip oriented at an angle relative to one another. The data in table 1 of the main paper show that high resolution imaging without artifacts was only accomplished with probes consisting of single tubes that had not been previously buckled.

The TEM images also show the presence of a low density contaminant coating on the probes. Evidence suggests that this material is deposited by silicone oil outgassing from the “gel-pack” in which most of the probes were stored.[11] This is supported by the significant amount of movement of this contaminant over the nanotube observed during TEM imaging. We have found via TEM imaging that gel-free clamshell tip wafer enclosures deposit about an order-of-magnitude less contamination on silicon AFM probes than gel-pack enclosures. This will be important for those wishing to perform dip pen nanolithography or nanotube probe functionalization. However, the contaminant had a limited effect for AFM imaging in air.

References

---

[1] Dai, H.; Hafner, J.H.; Rinzler, A.G.; Colbert, D.T.; Smalley, R.E. *Nature* **1996,** *384*, 147-150.

[2] Wong, S.S.; Harper, J.D.; Lansbury, P.T.; Lieber, C.M.:*J. Am. Chem. Soc.* **1998,** *120*, 603-604.

[3] Hafner, J.H.; Cheung, C.-L.; Lieber, C.M. *Nature* **1999,** *398*, 761-762.

[4] Hafner, J.H.; Cheung, C.L.; Lieber, C.M. *J. Am. Chem. Soc.* **1999**, 121, 9750-9751.

[5] Cooper, E.B.; Manalis, S.R.; Fang, H.; Dai, H.; Minne, S.C.; Hunt, T.; Quate, C.F. *Appl. Phys. Lett.* **1999,** *75*, 3566-3568.

[6] Li, Y.; Kim, W.; Zhang, Y.; Rolandi, M.; Wang, D.; Dai, H. *J. Phys. Chem. B* **2001,** *105*, 11424-11431.

[7] Wong, S.S.; Joselevich, E.; Wooley, A.T.; Cheung C.-L.; Lieber, C.M.:*Nature* **1998,** *394*, 52-55.

[8] Cheung, C.-L.; Hafner, J.H.; Odom, T.W.; Kim, K.; Lieber, C.M.:*Appl. Phys. Lett.* **2000**, *76*, 3136-3138.

[9] Hafner, J.; Rice University, private communication, March 2002.

[10] Snow, E.S.; Campbell, P.M.; Novak, J.P. *Appl. Phys. Lett.* **2002**, *80*, 2002-2004.

[11] Lo, Y.S.; Huefner, N.D.; Chan, W.S.; Dryden, P.; Hagenhoff, B.; Beebe, T.P. *Langmuir* **1999**, 15, 6522-6526.

J. Phys. Chem. B **2004,** *108,* 13613−13618

Influence of Elastic Deformation on Single-Wall Carbon Nanotube Atomic Force Microscopy Probe Resolution

Ian R. Shapiro,[†] Santiago D. Solares,[‡,§] Maria J. Esplandiu,[†,⊥] Lawrence A. Wade,[||] William A. Goddard,[*,†,§] and C. Patrick Collier[*,†]

Jet Propulsion Laboratory and Departments of Chemistry, Chemical Engineering, and Applied Physics, California Institute of Technology, Pasadena, California 91125

Received: May 14, 2004

We have previously reported that 4−6 nm diameter single-wall carbon nanotube (SWNT) probes used for tapping-mode atomic force microscopy (AFM) can exhibit lateral resolution that is significantly better than the probe diameter when prone nanotubes are imaged on a flat SiO_2 surface. To further investigate this phenomenon, accurate models for use in atomistic molecular dynamics simulations were constructed on the basis of transmission electron microscopy (TEM) and AFM data. Probe−sample interaction potentials were generated by utilization of force fields derived from ab initio quantum mechanics calculations and material bulk and surface properties, and the resulting force curves were integrated numerically with the AFM cantilever equation of motion. The simulations demonstrate that, under the AFM imaging conditions employed, elastic deformations of both the probe and sample nanotubes result in a decrease of the apparent width of the sample. This behavior provides an explanation for the unexpected resolution improvement and illustrates some of the subtleties involved when imaging is performed with SWNT probes in place of conventional silicon probes. However, the generality of this phenomenon for other AFM imaging applications employing SWNT probes remains to be explored.

Introduction

To date, numerous papers have described the preparation of both multiwall and single-wall carbon nanotube (SWNT) atomic force microscopy (AFM) probes.[1−5] SWNT probes offer topographic imaging resolution superior to that of conventional silicon AFM tips, due to their unique chemical and mechanical properties, high aspect ratios, and molecular-scale dimensions.[6−10] In a recent publication we have described an efficient SWNT probe fabrication methodology and correlated the structures [acquired by transmission electron microscopy (TEM)] of 14 probes with the quality of AFM images they produced when imaging a prone SWNT sample.[11] By comparing the observed AFM resolution with the diameter of the probe nanotube measured from the TEM image, we found that the lateral resolution is on average 1.2 times the nanotube probe diameter. This value approaches the expected ideal ratio of unity in the absence of thermal vibrations and bending effects of the probe.[12]

Surprisingly, we have found that for some cases the apparent lateral resolution of the probe nanotube was actually *better* than expected on the basis of its diameter. In one case (shown in Figure 6 of ref 11), which forms the basis for the computational work presented here, we found that the lateral resolution from a 5.5 nm diameter SWNT probe was 1.2 nm, just 22% of the probe diameter. Here and in previous investigations, we define the lateral resolution of a SWNT probe as the difference between the measured height of a sample, which can be determined to high precision with AFM, and the measured diameter (full width at the noise floor), as outlined in Figure 1. In an ideal case, the limiting resolution equals the diameter of the probe. This simplified model, in which the probe and sample are considered to be incompressible objects, has commonly been used to describe AFM resolution.[2,4,5] However, simple geometrical arguments alone cannot explain the subdiameter resolution we observed. The potential for SWNT AFM probes to be used as common research tools requires a more thorough understanding of how the physical, chemical, and mechanical properties of SWNT probes affect image resolution.

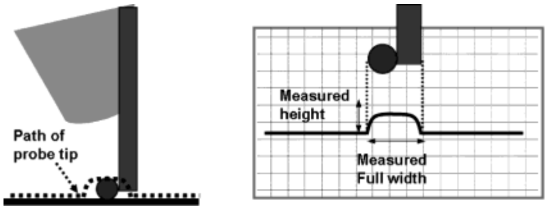

Figure 1. Schematic illustration of the relationship between probe diameter and lateral resolution. The left panel shows a model for a SWNT probe imaging a prone nanotube on a flat surface. The right panel shows the resulting cross-sectional profile, from which the width and height of the imaged nanotube are measured. In this simple geometric model, the full width is equal to the sum of the diameters of the probe and sample nanotubes.

To this end, we present here a quantitative atomistic molecular dynamics investigation of SWNT AFM probe behavior in the context of tapping-mode topographic imaging. The dimensions of the probes and samples are on the order of 1−50 nm, placing them within the range of atomistic simulations. To elucidate the actual tip−sample interactions that give rise to the observed phenomena, we have used TEM−AFM correlation data[11] to construct realistic molecular models of an open-ended SWNT probe interacting with a prone SWNT sample on a flat hydroxyl-

---

[*] Corresponding authors: e-mail collier@caltech.edu (C.P.C.), wag@wag.caltech.edu (W.A.G.).

[†] Department of Chemistry.

[‡] Department of Chemical Engineering.

[§] Materials and Process Simulation Center.

[||] Department of Applied Physics and Jet Propulsion Laboratory.

[⊥] Current address: Departament de Quimica, Universitat Autonoma de Barcelona, Barcelona, Spain.

10.1021/jp047937x CCC: $27.50

TABLE 1: Tapping-Mode AFM Parameters Used for Numerical Simulations

cantilever spring constant	$k = 4.8$ N/m
cantilever quality factor	$Q = 150$
cantilever resonant frequency	$\omega/2\pi = 47.48$ kHz
free air oscillation amplitude	$A_0 = 39$ nm
amplitude set-point	$A_{sp} = 15.4$ nm
excitation force	$F_0 = 1.25$ nN

terminated silicon surface. These models were used to generate accurate potential curves at different positions of the probe relative to the sample. Integration of the resulting forces into the equation of motion for an oscillating cantilever yielded simulated topographic cross-section profiles that corroborate the experimental results. These simulations indicate that, under the AFM conditions employed, both probe bending and localized deformations of the probe and sample SWNTs strongly influence the topographic profile measured with AFM. The reversible elastic nature of these deformations is demonstrated both experimentally and in simulations.

Methods

Fabrication, characterization, and imaging with SWNT AFM probes has been described previously.[11] The effective lateral resolution of each probe was obtained by imaging, under ambient conditions in air, a carbon nanotube lying prone on a flat native-oxide silicon surface. To acquire accurate sample height and width measurements by use of amplitude-modulated AFM, it was necessary to first carefully calibrate the response of the system over a wide range of operational parameters, most importantly, the oscillation amplitude of the SWNT probe. For example, to understand the effects that vertical compression of a sample nanotube by the AFM probe had on the lateral resolution, repeated measurements of the sample nanotube height as a function of probe oscillation amplitude were performed for both conventional silicon and SWNT AFM tips. In all cases, the driving amplitudes employed were kept below the limit corresponding to a 10% reduction in the apparent height of the sample nanotube due to compression. In addition, we measured force calibration curves, which consist of scans of the damped oscillation amplitude as a function of the average tip−sample separation for a given cantilever driving force. The force calibration curves revealed the presence of coexisting attractive and repulsive tip−sample interaction regimes.[13,14] Bistable switching of the cantilever oscillation between the two regimes manifests itself as sudden changes in the observed sample height and width.[15] In general, we avoided these amplitude instabilities and the concomitant experimental artifacts by operating the AFM cantilever with a driving force sufficient to give a free-air oscillation amplitude greater than 20 nm. Consequently, all AFM data presented here can be considered in the repulsive regime or "intermittent contact" mode.

The simulation of the AFM tip motion was carried out by integration of the equation of motion for a damped harmonic oscillator at each AFM scan point on the sample, with the experimental parameter values contained in Table 1:

$$m\frac{\mathrm{d}^2 z(Z_c, t)}{\mathrm{d}t^2} = -kz(Z_c, t) + m\frac{\omega_0}{Q}\frac{\mathrm{d}z(Z_c, t)}{\mathrm{d}t} + F_{ts}(z_{ts}) + F_0 \cos(\omega t) \quad (1)$$

where $z(Z_c, t)$ is the instantaneous tip position with respect to its average position (Z_c), k is the harmonic force constant for the displacement of the tip with respect to its equilibrium rest position, m is the effective mass, $\omega_0 = \sqrt{k/m}$, the free resonant frequency, Q is the quality factor, z_{ts} is the instantaneous tip position *with respect to the sample*, $F_{ts}(z_{ts})$ the calculated tip−sample interaction force, and $F_0 \cos(\omega t)$ is the oscillating driving force applied to the cantilever.

The use of this equation to describe the tip motion approximates the SWNT tip−cantilever ensemble as a point-mass harmonic oscillator. Nevertheless, this model has been used extensively for numerical treatment of tapping-mode AFM with conventional probes. Although the actual dynamics of the oscillating cantilever in the presence of the probe−sample interactions are nonlinear, the validity of the harmonic approximation for modeling conventional tapping-mode AFM imaging in air has been demonstrated with both theory and experiment for the range of parameters used here.[13,16−19]

Prior to integrating eq 1 we obtained the required tip−sample interaction forces using atomistic models, as explained in detail below. All molecular dynamics (MD) simulations were carried out with Cerius2 molecular simulations software (Accelrys, San Diego, CA). The MD force-field parameters were optimized by fitting the material bulk and surface properties such as elasticity moduli, vibrational frequencies, and surface geometry both to experimental data and to rigorous quantum mechanics calculations on clusters representative of the silicon and graphene systems under study. Equation 1 was integrated by use of the Verlet algorithm to fourth-order accuracy for the tip position and second-order accuracy for the tip velocity.[20]

Realistic atomistic models were constructed for the SWNT probe used for tapping-mode AFM imaging. Every effort was made to match the model structures and simulation conditions as closely as possible to corresponding experimental values, including the nanotube probe diameter, length, angle relative to the substrate normal, and the fine structure at the probe end. All silicon surfaces were (100) and were terminated with hydroxyl groups. The probe was a (40,40)[21] armchair SWNT (5.4 nm diameter, 45 nm length, with 5 nm of fixed atoms at one end of the probe to simulate its attachment site at the AFM tip) constructed from approximately 25 000 carbon atoms. The sample was a (16,16) armchair SWNT (2.2 nm diameter, 10 nm length) constructed from approximately 2600 carbon atoms. The sample SWNT was kept fixed at both ends during the calculations to simulate a very long nanotube, which is unlikely to displace laterally during AFM tapping. Similar models were generated for a conventional silicon tip interacting with the sample nanotube. Several of these models are shown in Figure 2.

The tip−sample interaction potentials were constructed by vertically approaching the sample with the probe nanotube at 0.05 nm intervals, at each point optimizing the system geometry by minimization of the potential energy (additional calculations performed at 300 K showed that the potentials did not significantly change with inclusion of thermal vibrations at room temperature; see Supporting Information). The gradient of this energy−position function with respect to the vertical tip position is the tip−sample interaction force.

To reduce the computational cost of the molecular simulations, each model of a nanotube on the surface included only a small section of the silicon surface, sufficient to obtain an accurate description of the SWNT probe interactions with the sample. This does not give an accurate description of the interaction of the tip with the silicon surface for the cases in which the SWNT tip deforms and slips against one side of the sample nanotube and makes contact with the underlying

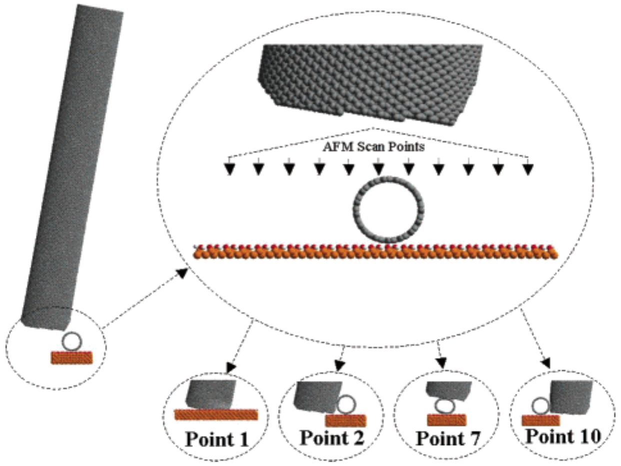

Figure 2. Illustration of the models used to construct the tip−sample interaction profile. The models were constructed on the basis of experimental TEM and AFM data. The final tip position during the AFM scan is shown for four of these points. The corresponding force curves are shown in Figure 3.

substrate. To correct this, another model was constructed *without* a sample nanotube on the substrate to obtain the interaction forces between the tip and the bare silicon surface. The deformation of the tip was considered in all cases when the relative position of the surface and the end of the tip was calculated for each scan point.

This procedure provides a discrete set of points, and so regression analysis with simple functional forms (e.g., polynomials or functions of the form $1/r^n$) was performed in order to obtain continuous force−position curves, which can be programmed easily into the AFM dynamics integration code. The forces for a given vertical position of the tip may have different values, depending on whether the tip has slipped relative to the sample SWNT. This was accounted for during the construction of the force−position curves and incorporated into the integration of the cantilever equation of motion.

Results and Discussion

A series of 11 curves showing probe−sample force versus height were generated at evenly spaced points along the line perpendicular to the axis of the sample nanotube. The separation between adjacent points was 1 nm. Figure 2 shows the location of the 11 scan points relative to the sample nanotube, and four of the corresponding tip−sample force curves are shown in Figure 3 (all 11 energy-position curves, from which these force curves were obtained by differentiation, are provided in the Supporting Information). The abscissa on all graphs in Figure 3 corresponds to the distance between the lowest atom on the SWNT tip and the highest atom of the Si(100)−OH surface. Negative values on this axis correspond to elastic deformations in nanotube and surface geometry, including local deformation of the probe, as well as slight deformation of the Si−OH surface.

Each of the 11 probe−sample force curves generated along the scan line was then inserted into eq 1 and integrated for the average tip positions relative to the substrate (Z_c) ranging from 50 to 0 nm, by use of actual imaging parameter values.[11] For each scan point and tip position, eq 1 was integrated numerically for 0.02 s with a 0.1 ns integration step (to fourth-order accuracy with respect to the time step size) to determine the oscillation amplitude of the cantilever as a function of its vertical position [the initial tip position was set equal to its equilibrium position, i.e., $z(Z_c, 0) = 0$, and the initial velocity was set to zero in all cases]. This numerical procedure is analogous to acquiring a “force calibration curve” for each scan point in Figure 2.

The result of these calculations was a curve showing the cantilever equilibrium oscillation amplitude as a function of the average vertical position of the tip for each point along the scan direction. Two of these curves are shown as insets in Figure 5. The simulated cross-section trace in Figure 5 was then constructed by plotting the locus of tip position values which maintained the oscillation amplitude at the set-point value of 15.4 nm. Note that the average tip−sample separation for each scan point is given relative to the value obtained when imaging the bare silicon oxide substrate.

The construction of tip−sample interaction force curves through molecular simulations of large finite systems underestimates the long-range attractive forces present in the system. This is because the calculation of nonbonded interaction energies between pairs of atoms is generally limited to a cutoff radius on the order of 1 nm or less to reduce the cost of the computation (the number of nonbonded interactions, which scales with the square of the number of atoms in the simulation, can account for over 90% of the computation costs of a typical system). Underestimating the long-range attractive forces, and hence the region of positive force gradient, can alter the predicted regions of amplitude bistability.[13] However, at the free oscillation amplitude employed here, $A_0 = 39$ nm, the average force will be determined almost exclusively by the repulsive part of the tip−sample interaction potential,[16] and thus the underestimation of the attractive contribution will have negligible influence on the simulated topographic profile.

Under ambient conditions, a thin film of water is adsorbed on hydrophilic surfaces such as SiO_2. The formation of a meniscus or liquid bridge between the surface and the probe will result in an additional attractive capillary force that depends on probe−sample distance.[22] We did not include the effects of adsorbed water in our model. We do not expect that inclusion of these effects will significantly change the nanoscopic interactions between the probe and sample nanotubes predicted by the simulations. Future work will address this issue.

Simple models of AFM resolution assume that the probe is a rigid, incompressible cylinder with a flat or hemispherical end. In practice this is not the case. High-magnification TEM images show that the ends of the probe nanotubes are generally open due to ablation from an electrical etching procedure used to shorten the nanotube probes to useful lengths.[2,4] Purely geometric arguments suggest that an open-ended tube with protruding asperities could, for extremely low-relief samples, provide resolution comparable to the asperity diameter rather than the full diameter of the probe, in direct analogy to results published for silicon probes.[23] However, probe asperities are unlikely to be important when imaging a sample nanotube that has a diameter (height above the surface) comparable to that of the probe.

The Young’s modulus of SWNTs is approximately 1.25 TPa along the tube axis.[24] Because of this very high stiffness, only a small amount of longitudinal compression of the tube occurs during AFM imaging. However, Snow et al.[12] have shown that SWNT probes are susceptible to bending due to their high aspect ratio if not oriented vertically relative to a surface. Image artifacts from bending can be minimized by shortening the nanotube probe so that it protrudes less than 100 nm beyond the supporting silicon tip.

While SWNTs have exceptional longitudinal stiffness, radially they are far more compliant,[25] a characteristic that permits localized deformation of the nanotube walls. The likelihood of deformation is further increased due to the structural discontinu-

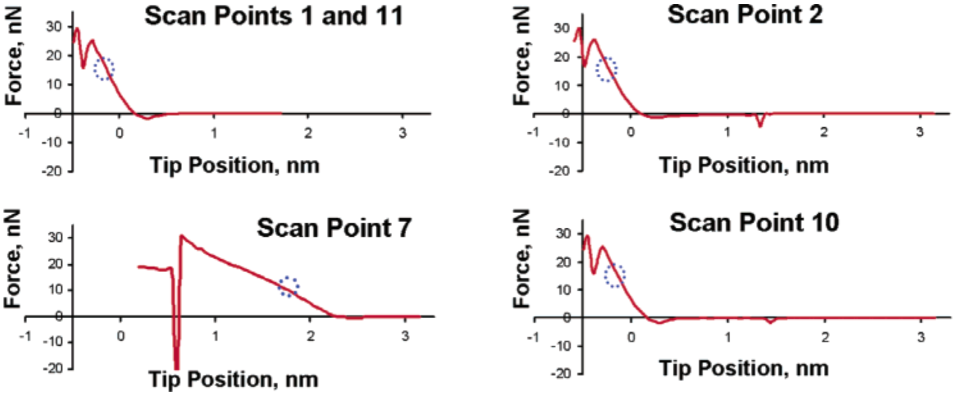

Figure 3. Tip−sample force curves calculated for four of the 11 scan points shown in Figure 2. The abscissa on all graphs corresponds to the distance between the lowest atom on the SWNT tip and the highest atom of the Si(100)−OH surface. The small blue circle in each plot indicates the lowest position that the probe tip reached during the subsequent AFM imaging simulation.

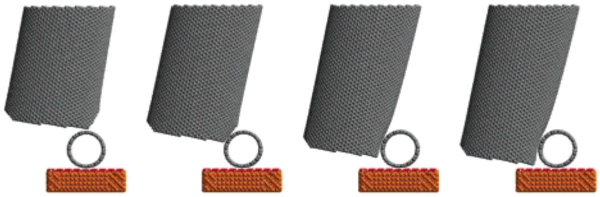

Figure 4. Illustration of the slipping phenomenon of the SWNT probe past the SWNT sample for scan point 3. Both bending along the length of the probe and local deformation contribute to slipping. The picture shows that the simulated probe is more susceptible to deformation, although the sample nanotube does deform slightly. This is due to the larger diameter of the probe (5.4 vs 2.2 nm) and the fact that its end is opened, which decreases its radial rigidity.

ity at the opened end of the nanotube probe. The susceptibility of nanotubes to radial deformation is predicated upon two competing effects: the energy cost associated with strain of the nanotube as it is deformed from its equilibrium cylindrical geometry, and the stabilization that a compressed nanotube gains due to increased interlayer van der Waals attractions. These two competing effects scale in opposite directions with increased nanotube diameter, such that larger SWNTs are easier to deform radially than smaller diameter tubes.[26] We have previously observed that SWNTs attached to silicon AFM tips via the "pick-up" method tend to be 4−6 nm, which is larger than the tubes observed lying prone upon the pick-up substrate (1−3 nm).[11] We postulated that the increase in net binding energy with larger diameter nanotubes stems from the interplay between van der Waals forces and the geometric stiffness of a nanotube. The resulting radial "softness" of these larger nanotubes not only increases the energy with which they bind to a silicon probe during pick-up but also has significant implications when they are subsequently used for AFM imaging.

Our molecular dynamics simulations show lateral slipping of the probe nanotube relative to the sample nanotube, due both to bending along the length of the probe and to localized radial deformation of the probe and sample at the point of contact (illustrated in Figure 4 and Supporting Information). This behavior is a function of the structures and relative orientations of the probe and sample nanotubes, the applied tip−sample force, and the position (in the $x-y$ plane) of the probe nanotube relative to the sample nanotube. The smaller the $x-y$ distance between the center of the probe tube and the axis of the sample tube, the larger the force required to deform the nanotubes and cause them to slip past one another. That is, when the probe presses on the edge of the sample nanotube, a smaller amount of force is required to cause it to slip laterally than when it presses on the crown of the sample nanotube. The simulations show this deformation behavior to be completely reversible and elastic (images illustrating reversibility are provided in the Supporting Information). Experimentally, the elasticity is demonstrated by the fact that we have not observed the topographic cross sections to change significantly during imaging at a given amplitude set-point, and the TEM images taken of each probe after AFM imaging show no alterations of the nanotube structure, such as kinks or buckles.

This lateral slipping and deformation of the probe nanotube explains the observation of sub-probe-diameter effective resolution. In amplitude−feedback tapping-mode AFM, modulation of the cantilever oscillation amplitude depends on the average strength of the tip−sample forces.[27] The AFM controller adjusts the extension of the z-piezoelectric element in order to hold the amplitude of the cantilever oscillation at the fixed value designated by the amplitude set-point (an independent variable set by the user). The resulting z-piezo voltage corrections are converted to units of length and output as the topographic height data. If the probe and sample deform negligibly under the associated tapping forces, the sample height can be measured accurately to within the precision of the piezoelectric element, typically <1 Å. However, if either material is significantly deformable, the resultant z-piezo data represents a more complex convolution of probe and sample structure.

The simulations conducted here indicate that when the probe SWNT is tapping on an edge of the sample SWNT, the subsequent repulsive forces deform *both* nanotubes sufficiently to allow them to slip past one another without significantly influencing the cantilever oscillation amplitude. In fact, when the very edges of the probe and sample tubes come into contact, the net tip−sample force is actually attractive rather than repulsive, due to the large area of favorable contact between the graphitic surfaces. This is illustrated in the force curves for scan points 2 and 10 by the fact that the net force is negative between the two local minima, corresponding to the region in which the probe and the sample are slipping past one another. Once lateral slipping takes place, the resulting tip−sample interaction is dominated by the repulsive forces between the probe SWNT and the Si/SiO_2 surface. Thus, for that particular $x-y$ position, the AFM controller does not "see" the sample nanotube. Only when the probe SWNT is positioned closer to the crown of the prone sample SWNT are the interaction forces between the probe and sample nanotubes high enough to cause sufficient damping of the cantilever oscillation amplitude. At scan point 7, which corresponds to the probe tapping on the crown of the sample nanotube, no slipping can take place under

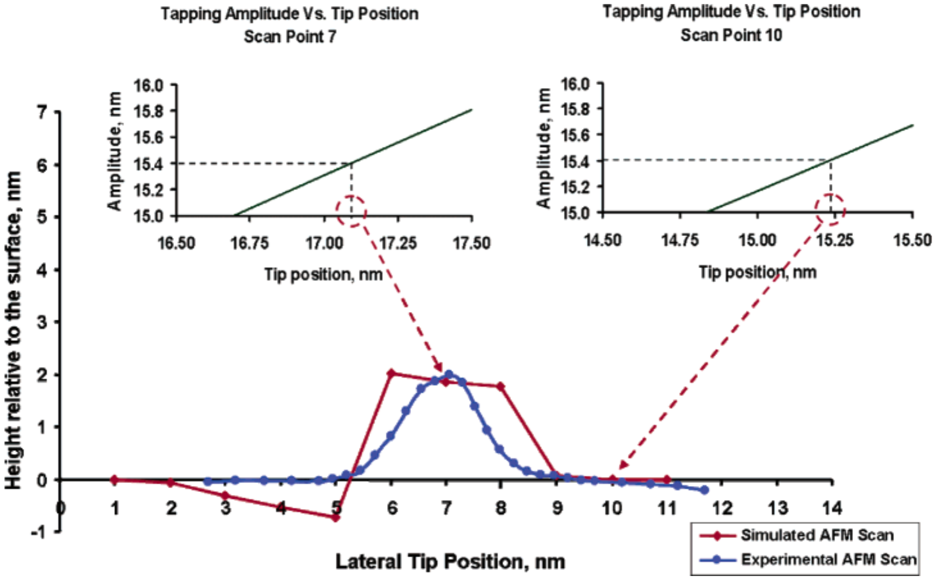

Figure 5. Schematic depiction of the construction of an AFM scan from molecular and AFM dynamics simulations. The two inset amplitude−distance curves illustrate how the measured height is obtained for each scan point at an amplitude set-point of 15.4 nm. The resulting AFM cross-sectional height is given relative to the average tip separation from the bare SiO_2 surface. The horizontal axis corresponds to the scan points shown in Figure 2. For comparison, the cross section from experimental data has been overlaid on the same scale with its center point arbitrarily positioned to match up with the center of the simulated cross section.

the imaging conditions given in Table 1, because the maximum tip−sample repulsive force does not exceed the necessary threshold, ∼30 nN. Here, the cantilever amplitude is damped by the sample nanotube and the AFM records the interaction. The net result is that the topographic data indicates an apparent nanotube width that is smaller than the sum of the probe and sample SWNT diameters.

A quantitative representation of this phenomenon is illustrated in Figure 5. The lower half of the figure shows the effective cross section of a sample nanotube, calculated from the MD and AFM dynamics simulations, obtained when a SWNT probe is used under the repulsive tapping conditions given in Table 1. This scan shows two important features that are also observed experimentally. First, the apparent probe resolution for this simulation is 2.0 nm, 37% of the probe diameter. Additionally, the simulated cross section is asymmetric, which is a direct consequence of the specific SWNT probe geometry, particularly the tilt angle, that favors probe−sample slipping more on one side of the sample than on the other.

In contrast, MD simulations have shown that a conventional silicon probe does not slip under the same imaging conditions. This is because the rigidity of the silicon probe requires higher forces to induce deformation, while the larger radius of curvature of the probe tip actually generates smaller lateral forces compared to a SWNT probe. The different behavior is also due to the chemical properties of crystalline silicon, which strongly influence the surface−surface interactions with the SWNT sample, as well as the attractive van der Waals forces between the larger silicon tip and the silicon surface. These two parameters in particular, probe compressibility and adhesion forces, are transformed in a highly nonlinear way by the response of the oscillating tip.[28] Thus, SWNT probes perform in a fundamentally different manner than silicon probes, not merely when imaging prone carbon nanotubes but for a variety of samples.

We have also simulated a smaller diameter SWNT probe since previous reports have described nanotube probes in the 1−3 nm diameter range.[1,2,4,7] Smaller diameter nanotube probes should be far less susceptible to localized radial deformation, due to their increased resistance against compression (as seen with the sample nanotube, Figure 4). However, the bending mode along the length of a thinner probe is actually softer, since the flexural rigidity scales as r^4.[29] The probe was a (16,16) armchair SWNT (2.2 nm diameter, 20 nm length) that had approximately the same aspect ratio as the larger 5.4 nm probe used in this study. As before, the probe nanotube was oriented at 15° relative to the surface normal and the sample nanotube was 2.2 nm in diameter and 10 nm in length. Images from the simulation are incorporated in the Supporting Information and show that slipping also occurs for the thinner probe when tapping on the edge of the sample nanotube. For this probe, the slipping is almost entirely due to bending and not to local deformation. The corresponding tip−sample force curve indicates that the force opposing the slipping motion of the probe was negligible.

Dekker and co-workers[30] have reported previously that as a function of driving amplitude in tapping-mode imaging, a conventional silicon AFM probe can vertically compress a 1.4 nm single-wall nanotube lying on a flat surface, resulting in a decreased apparent *height*. This experimental observation is consistent with previously reported experimental measurements and molecular dynamics simulations, which described radial deformation of 1−3 nm single-wall carbon nanotubes by both van der Waals forces and external static loads.[31−33] Here we show that in tapping-mode AFM, the associated forces deform the probe nanotube in addition to the sample, strongly influencing the subsequently measured effective *lateral* resolution.

Our molecular dynamics simulations confirm that some vertical compression of a prone sample nanotube occurs under standard tapping-mode AFM conditions, for both conventional silicon AFM probes and SWNT probes. However the simulations predict that this effect is, at most, 10% of the sample tube diameter for 1−3 nm SWNTs and occurs primarily when the probe nanotube is tapping on the crown of the sample nanotube (see, for example, point 7 in Figure 2). This corresponds well with our experimental calibration of sample tube compression under the tapping-mode operating parameters employed. The enhanced lateral resolution, on the other hand, is due to the highly localized deformation and bending of the probe nanotube along the edges of the sample nanotube, and is therefore not affected significantly by vertical compression.

Conclusion

By correlating experimental data with atomistic molecular dynamics simulations, we have characterized how the unique properties of SWNT AFM probes can strongly influence topographic imaging fidelity. Probe bending and mutual local deformation of both the probe and sample nanotubes under typical tapping-mode AFM forces can result in a reduction of the measured width of the sample tube, and consequently an ostensive improvement of the lateral resolution, to the extent that the resolution can appear to be better than expected from the measured diameter of the nanotube probe. We are interested in determining whether a similar improvement of apparent resolution is observed when imaging less compliant samples of different material composition, such as metallic or semiconducting nanoparticles.

Given the interest in nanoscale physical and biological phenomena, SWNT probes are likely to evolve into a more common research tool. A complete understanding of probe behavior in the context of atomic force microscopy is therefore critical. It is important to note that the lateral resolution reported here is an apparent value, arising from the simplified definition set forth in the Introduction, and was studied for the specific case of 4−6 nm diameter open-ended SWNT probes imaging 2−3 nm diameter SWNTs adsorbed on a flat surface. In practice, the resolving power of an AFM probe is dependent upon the experimental context. It is of particular importance to determine whether the observed deformation phenomenon results in a net gain or loss of structural information when SWNT probes are used to image soft nanoscale samples, such as biological macromolecules. The improvement in the apparent resolution due to deformation of the probe and sample nanotubes in this study was a consequence of the relatively high driving forces applied to the AFM cantilever. Tapping-mode AFM imaging performed in this repulsive regime with conventional probes has been shown to damage biomolecules.[14] In addition, resolution less than the probe diameter could complicate interpretation of AFM images quantitatively.

The combination of probe structure determination, characterization of imaging resolution, and simulated dynamic behavior described here has highlighted practical differences between carbon nanotube probes and conventional silicon probes. This work also underscores the usefulness of atomistic simulations in describing the dynamic nanoscale interactions involved in scanning probe microscopy.

Acknowledgment. We thank Professor Stephen Quake, Dr. Jordan Gerton, and Ms. Yuki Matsuda for essential discussions. I.R.S., M.J.E., and C.P.C. were supported by Caltech startup funds and by Arrowhead Research. S.D.S. and W.A.G. were supported by NSF-NIRT Grant CTS-0103002, and by the Microelectronics Advanced Research Corporation (MARCO) and its Focus Center on Function Engineered NanoArchitectonics (FENA). L.A.W. was supported by the Caltech President's Fund and NASA Contract NAS7-1407.

Supporting Information Available: Simulated energy−distance and force−distance curves, force-field parameters, effects of thermal vibrations, illustrations of bending and local deformation modes of a 5.4 nm diameter SWNT probe, of lateral slipping of a 2.2 nm diameter SWNT probe, and the elastic nature of nanotube deformation. This material is available free of charge via the Internet at http://pubs.acs.org.

References and Notes

(1) Cheung, C.-L.; Hafner, J. H.; Odom, T. W.; Kyoungha, K.; Lieber, C. M. *Appl. Phys. Lett.* **2000**, *76*, 3136.
(2) Wong, S. S.; Wooley, A. T.; Joselevich, E.; Cheung, C. L.; Lieber, C. M. *J. Am. Chem. Soc.* **1998**, *120*, 8557.
(3) Campbell, P. M.; Snow, E. S.; Novak, J. P. *Appl. Phys. Lett.* **2002**, *81*, 4586.
(4) Hafner, J. H.; Cheung, C. L.; Oosterkamp, T. H.; Lieber, C. M. *J. Phys. Chem. B* **2001**, *105*, 743.
(5) Choi, N.; Uchihashi, T.; Nishijima, H.; Ishida, T.; Mizutani, W.; Akita, S.; Nakayama, Y.; Ishikawa, M.; Tokumoto, H. *Jpn. J. Appl. Phys.* **2000**, *39*, 3707.
(6) Dai, H.; Hafner, J. H.; Rinzler, A. G.; Colbert, D. T.; Smalley, R. E. *Nature* **1996**, *384*, 147.
(7) Wong, S. S.; Woolley, A. T.; Odom, T. W.; Huang, J.-L.; Kim, P.; Vezenov, D. V.; Lieber, C. M. *Appl. Phys. Lett.* **1998**, *73*, 3465.
(8) Hafner, J. H.; Cheung, C. L.;. Wooley, A. T.; Lieber, C. M. *Prog. Biophys. Mol. Biol.* **2001**, *77*, 73.
(9) Stevens, R. M. D.; Frederick, N. A.; Smith, B. L.; Morse, D. E.; Stucky, G. D.; Hansma, P. K. *Nanotechnology* **2000**, *11*, 1.
(10) Nguyen, C. V.; Stevens, R. M. D.; Barber, J.; Han, J.; Meyyapan, M. *Appl. Phys. Lett.* **2002**, *81*, 901.
(11) Wade, L. A.; Shapiro, I. R.; Ma, Z.; Quake, S. R.; Collier, C. P. *Nano Lett.* **2004**, *4*, 725.
(12) Snow, E. S.; Campbell, P. M.; Novak, J. P. *Appl. Phys. Lett.* **2002**, *80*, 2002.
(13) García, R.; San Paulo, A. *Phys. Rev. B.* **1999**, *60*, 4961.
(14) San Paulo, A.; García, R. *Biophys. J.* **2000**, *78*, 1599.
(15) García, R.; San Paulo, A. *Phys. Rev. B.* **2000**, *61*, R13381.
(16) San Paulo, A.; García, R. *Phys. Rev. B.* **2002**, *66* R041406.
(17) San Paulo, A.; García, R. *Phys. Rev. B.* **2001**, *64*, 193411.
(18) Rodriguez, T. R.; García, R. *Appl. Phys. Lett.* **2002**, *80*, 1646.
(19) Cleveland, J. P.; Anczykowski, B.; Schmid, A. E.; Elings, V. B. *Appl. Phys. Lett.* **1998**, *72*, 2613.
(20) For an explanation of (*n*, *m*) designation, see Jeroen, W. G.; Wildoer, L. C.; Venema, A. G.; Rinzler, R.; Smally, E.; Dekker, C. *Nature* **1998**, *391*, 59.
(21) Frenkel, D.; Smit, B. *Understanding Molecular Simulation*; Academic Press: San Diego, CA, 2002; pp 69−71.
(22) García, R.; Calleja, M.; Rohrer, H. *J. Appl. Phys.* **1999**, *86*, 1898.
(23) Engel, A.; Müller, D. *Nat. Struct. Biol.* **2000**, *7*, 715.
(24) Krishnan, A.; Dujardin, E.; Ebbesen T. W.; Yianilos, P. N.; Treacy, M. M. J. *Phys. Rev. B* **1998**, *58*, 14013.
(25) Shen, W.; Jiang, B.; Han, B. S.; Xie, S.-S. *Phys. Rev. Lett.* **2000**, *84*, 3634.
(26) Gao, G.; Çağin, T.; Goddard, W. A. *Nanotechnology* **1998**, *9*, 184.
(27) García, R.; Perez, R. *Surf. Sci. Rep.* **2002**, *47*, 197.
(28) Lee, S. I.; Howell, S. W.; Raman, A.; Reifenberger, R. *Phys. Rev. B.* **2002**, *66*, 115409.
(29) Wilson, N. R.; Macpherson, J. V. *Nano Lett.* **2003**, *3*, 1365.
(30) Postma, H. W. C.; Sellmeijer, A.; Dekker, C. *Adv. Mater.* **2000**, *12*, 1299.
(31) Hertel, T.; Walkup, R. E.; Avouris, P. *Phys. Rev. B* **1998**, *58*, 13870.
(32) Li, C.; Chow, T.-W. *Phys. Rev. B* **2004**, *69*, 073401.
(33) Ruoff, R. S.; Tersoff, J.; Lorents, D. C.; Subramoney, S.; Chan, B. *Nature* **1993**, *364*, 514.

Supplemental information for J.Phys.Chem.B 2004, Vol. 108, 13613-13618.

Influence of Elastic Deformation on Single-Wall Carbon Nanotube AFM Probe Resolution

Ian R. Shapiro, Santiago D. Solares, Maria J. Esplandiu, Lawrence A. Wade, William A. Goddard, and C. Patrick Collier**

Supporting Information

Tables of force field parameters:

TABLE 1: Force Field Energy Expression

Total Energy	$E = E_{\text{bond stretch}} + E_{\text{angle bend}} + E_{\text{torsion}} + E_{\text{stretch-bend-stretch}} + E_{\text{stretch-stretch}} + E_{\text{van der Waals}}$ *
Bond Stretch Energy Type Harmonic	$E = \frac{1}{2} K_b (R - R_o)^2$
Bond Stretch Energy Type Morse	$E = D_o (e^{-\alpha(R-R_o)} - 1)^2$ where $\alpha = \sqrt{\frac{K_b}{2D_o}}$

Angle Bend Energy Theta Harmonic	$E = \frac{1}{2} K_\theta (\theta - \theta_o)^2$
Angle Bend Energy Cosine Harmonic	$E = \frac{1}{2 Sin^2 \theta_o} K_\theta (Cos\theta - Cos\theta_o)^2$
Torsion Energy Dihedral	$E = \frac{1}{2} K_t [1 - d_t Cos(n_t \phi)]$
Stretch-Bend-Stretch Energy R-Cosine	$E = (Cos\theta - Cos\theta_o)[C_{ij}(Rij - Rij_o) + C_{jk}(Rjk - Rjk_o)]$
Stretch-Stretch Energy R-R	$E = K_{ss}(Rij - Rij_o)(Rjk - Rjk_o)$
Van der Waals Energy Morse	$E = D_o(\chi^2 - 2\chi)$ where $\chi = e^{\frac{-\gamma}{2}(\frac{R}{R_o} - 1)}$
Van der Waals Energy Lennard-Jones 6-12	$E = D_o((\frac{R_o}{R})^{12} - 2(\frac{R_o}{R})^6)$

* The present study did not consider charged samples or probes; hence the energy expression does not include electrostatic energy terms.

TABLE 2: Force Field Atom Types

H_	Non-acid hydrogen
H___A	Acid hydrogen
C_3	SP^3 carbon
C_2G	SP^2 graphite carbon
O_3	SP^3 oxygen
Si0	Bulk silicon
SiS	Surface silicon
SiOH	Surface silicon connected to OH group
SiH	Surface silicon connected to H_

TABLE 3: Harmonic Bond Stretch Parameters

Atom 1	**Atom 2**	**K_b**	**R_o**
SiOH	O_3	700.0000	1.5870
O_3	H___A	500.0000	1.0000
C_3	H_	662.6080	1.1094
C_3	C_3	699.5920	1.5140
C_2G	H_	700.0000	1.0200
C_2G	C_3	739.8881	1.4860
H_	H_	700.0000	0.7500

TABLE 4: Morse Bond Stretch Parameters

Atom 1	**Atom 2**	***K_b***	***R_o***	***D_o***
SiOH	H_	382.3870	1.4830	92.6000
SiH	H_	382.3870	1.4830	92.6000
Si0	Si0	193.0936	2.3810	73.7000
SiOH	Si0	193.0936	2.3810	73.7000
SiH	Si0	240.0660	2.3810	73.7000
SiOH	SiOH	193.0936	2.3810	73.7000
SiH	SiH	193.0936	2.3810	73.7000
C_2G	C_2G	720.0000	1.4114	133.0000
SiS	Si0	193.0936	2.3810	73.7000
SiS	SiS	193.0936	2.3810	73.7000

TABLE 5: Angle Bend Parameters

Atom 1	**Atom 2**	**Atom 3**	**Type**	K_θ	θ_o
C_2G	C_2G	C_2G	Cosine harmonic	196.1300	120.0000
C_2G	C_2G	C_3	Cosine harmonic	196.1300	120.0000
C_3	C_2G	C_3	Cosine harmonic	188.4421	120.0000
C_2G	C_3	C_2G	Cosine harmonic	220.2246	109.4710
C_3	C_3	C_3	Cosine harmonic	214.2065	109.4710
C_3	C_2G	H_	Cosine harmonic	98.7841	120.0000
Si0	SiH	H_	Cosine harmonic	42.2500	115.1400
Si0	Si0	Si0	Cosine harmonic	31.2682	105.0467
C_3	C_3	H_	Cosine harmonic	117.2321	109.4710
C_2G	C_3	H_	Cosine harmonic	121.6821	109.4710
C_2G	C_3	C_3	Cosine harmonic	220.2246	109.4710
C_2G	C_2G	H_	Cosine harmonic	103.1658	120.0000
Any	O_3	Any	Theta harmonic	100.0000	104.5100
H_	SiOH	H_	Cosine harmonic	58.2560	110.9530
Si0	SiOH	O_3	Cosine harmonic	102.7429	109.4710
SiOH	SiOH	Si0	Cosine harmonic	31.2682	105.0467
SiOH	Si0	Si0	Cosine harmonic	31.2682	105.0467
SiOH	Si0	SiOH	Cosine harmonic	31.2682	105.0467
SiH	SiH	Si0	Cosine harmonic	31.2682	105.0467
Si0	SiH	Si0	Cosine harmonic	31.2682	105.0467
SiH	Si0	SiH	Cosine harmonic	31.2682	105.0467
SiS	Si0	Si0	Cosine harmonic	31.2682	105.0467
SiS	Si0	SiS	Cosine harmonic	31.2682	105.0467
Si0	SiOH	Si0	Cosine harmonic	31.2682	105.0467
SiOH	SiOH	O_3	Cosine harmonic	102.7429	109.4710
SiH	SiH	H_	Cosine harmonic	42.2500	115.1400

Si0	SiS	Si0	Cosine harmonic	31.2682	105.0467	100
SiS	SiS	Si0	Cosine harmonic	31.2682	105.0467	
O_3	SiOH	H_	Cosine harmonic	57.6239	109.4710	

TABLE 6: Torsion Parameters

Atom 1	Atom 2	Atom 3	Atom 4	K_t	n_t	d_t
C_2G	C_2G	C_2G	C_2G	85.1200	2.0000	1.0000
Any	C_2G	C_2G	Any	100.0000	2.0000	1.0000
Any	C_2G	C_3	Any	2.0000	3.0000	-1.0000
Any	C_3	C_3	Any	2.0000	3.0000	-1.0000
Any	SiOH	O_3	Any	2.0000	3.0000	-1.0000

TABLE 7: Stretch-Bend-Stretch Parameters

Atom 1	Atom 2	Atom 3	Rij	Rjk	θ_o	C_{ij}	C_{jk}
Si0	Si0	Si0	2.3810	2.3810	109.4712	-14.8184	-14.8184

TABLE 8: Stretch-Stretch Parameters

Atom 1	Atom 2	Atom 3	K_{ss}	Rij_o	Rjk_o
Si0	Si0	Si0	3.6001	2.3810	2.3810

TABLE 9: van der Waals Parameters

Atom 1	Atom 2	Type	D_o	R_o	γ
H_	H_	Morse	0.018145	3.56979	10.70940

H___A	H___A	LJ 6-12	0.000099	3.19499	N/A
C_3	C_3	LJ 6-12	0.146699	3.98300	N/A
C_2G	C_2G	Morse	0.098999	3.993999	10.96300
O_3	O_3	LJ 6-12	0.095700	3.404599	N/A
Si0	Si0	LJ 6-12	0.310000	4.269999	N/A
SiS	SiS	LJ 6-12	0.310000	4.269999	N/A
SiOH	SiOH	LJ 6-12	0.310000	4.269999	N/A
SiH	SiH	LJ 6-12	0.310000	4.269999	N/A
C_2G	H_	Morse	0.034710	3.744610	12.25614
SiOH	C_2G	LJ 6-12	0.175186	4.132000	N/A
Si0	C_2G	LJ 6-12	0.175186	4.132000	N/A
SiH	C_2G	LJ 6-12	0.175186	4.132000	N/A
SiS	C_2G	LJ 6-12	0.175186	4.132000	N/A
O_3	C_2G	LJ 6-12	0.097336	3.699299	N/A

The original parameters used to create these force fields were developed in the Materials and Process Simulation Center (California Institute of Technology).[1,2,3] Additional parameters were added to study mixed systems (containing silicon, graphitic systems, oxygen and hydrogen) by applying arithmetic and/or geometric combination rules to existing parameters, by quantum mechanics calculations conducted by Weiqiao Deng, Richard Muller and William A. Goddard III or by using generic terms from the Dreiding force field.[4]

Energy-position and force-position curves from MD simulations:

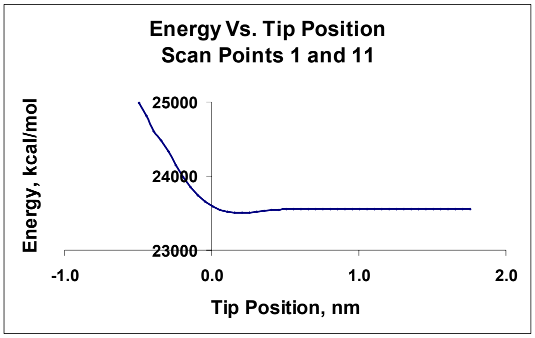

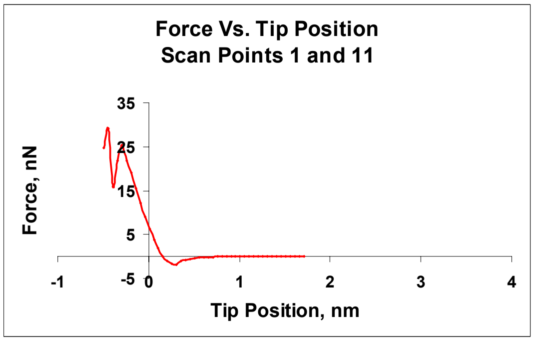

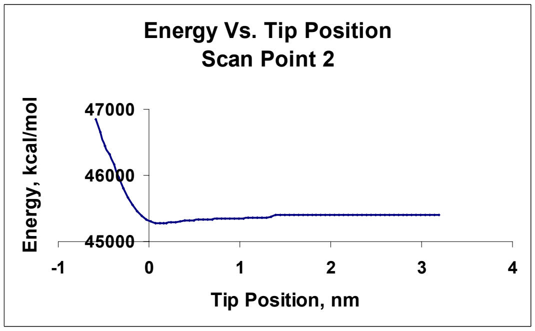

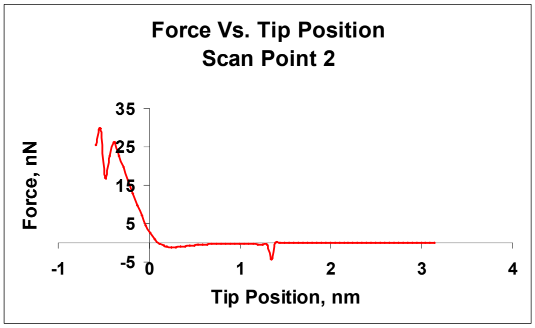

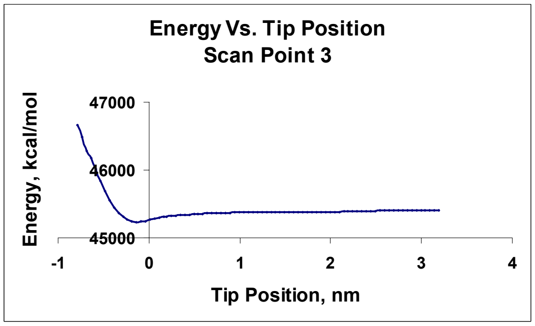

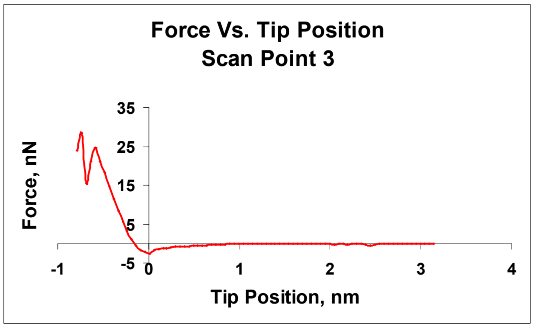

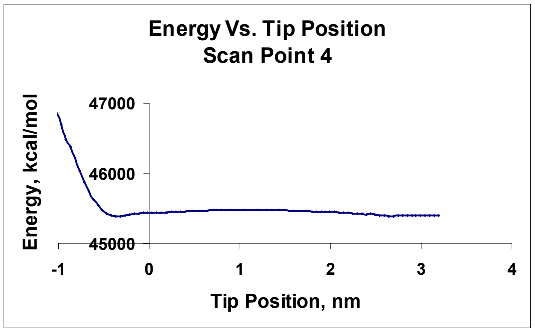

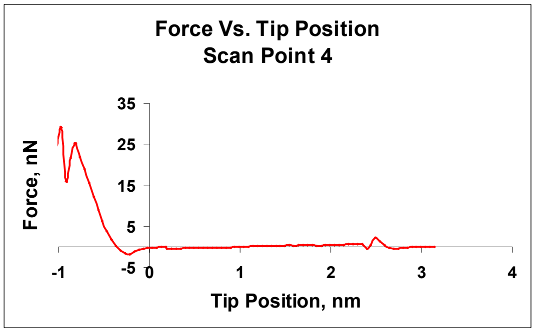

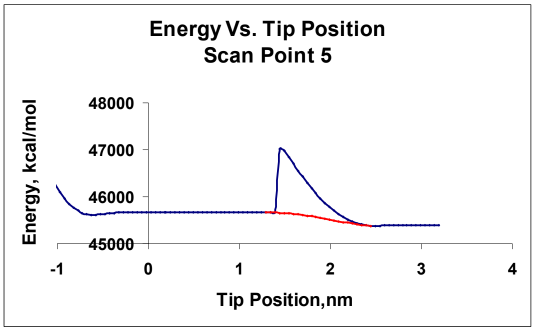
Energy Vs. Tip Position
Scan Point 5
Energy, kcal/mol
48000
47000
46000
45000
-1
0
1
2
3
4
Tip Position,nm

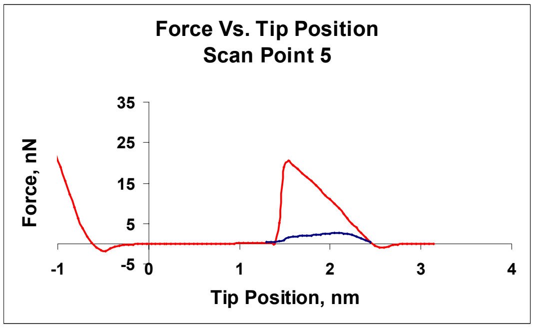
Force Vs. Tip Position
Scan Point 5
Force, nN
35
25
15
5
-5
-1
0
1
2
3
4
Tip Position, nm

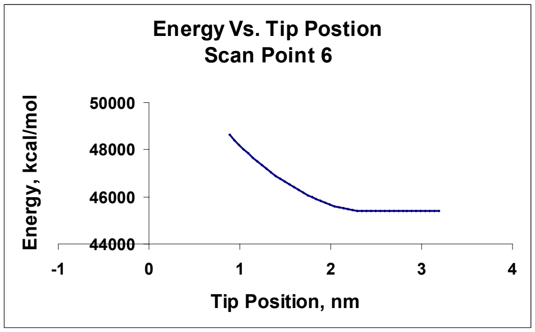
Energy Vs. Tip Postion
Scan Point 6
Energy, kcal/mol
50000
48000
46000
44000
-1
0
1
2
3
4
Tip Position, nm

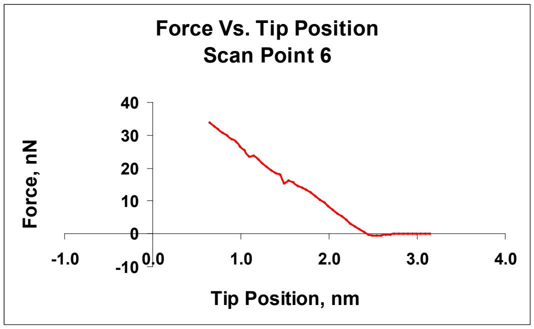
Force Vs. Tip Position
Scan Point 6
Force, nN
40
30
20
10
0
-10
-1.0
0.0
1.0
2.0
3.0
4.0
Tip Position, nm

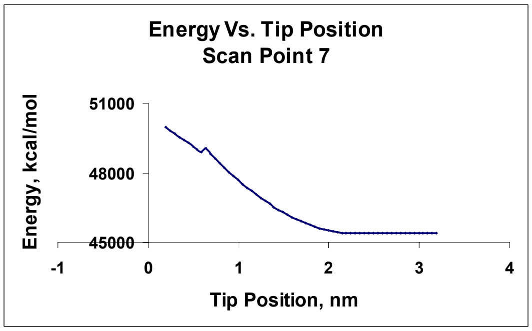
Energy Vs. Tip Position
Scan Point 7
Energy, kcal/mol
51000
48000
45000
-1
0
1
2
3
4
Tip Position, nm

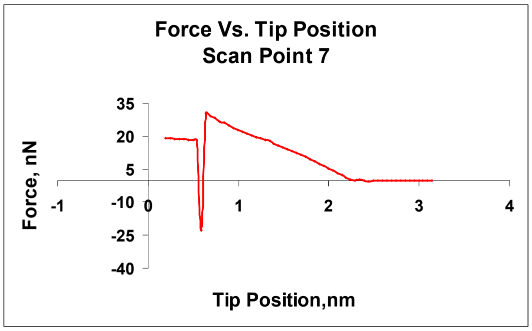
Force Vs. Tip Position
Scan Point 7
Force, nN
35
20
5
-10
-25
-40
-1
0
1
2
3
4
Tip Position,nm

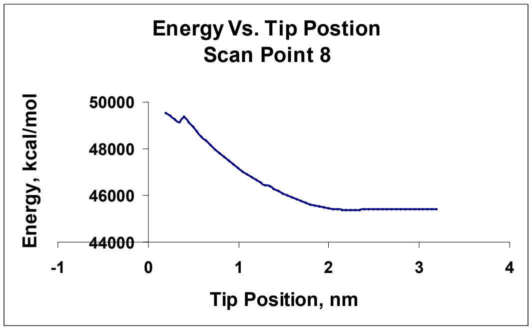
Energy Vs. Tip Postion
Scan Point 8
Energy, kcal/mol
50000
48000
46000
44000
-1
0
1
2
3
4
Tip Position, nm

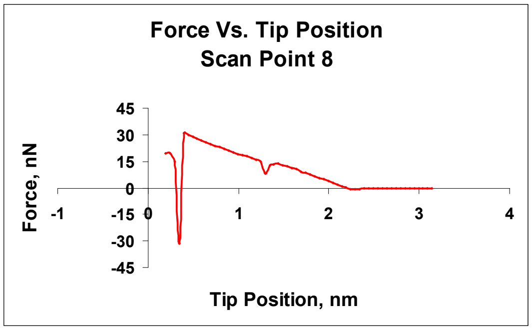
Force Vs. Tip Position
Scan Point 8
Force, nN
45
30
15
0
-15
-30
-45
-1
0
1
2
3
4
Tip Position, nm

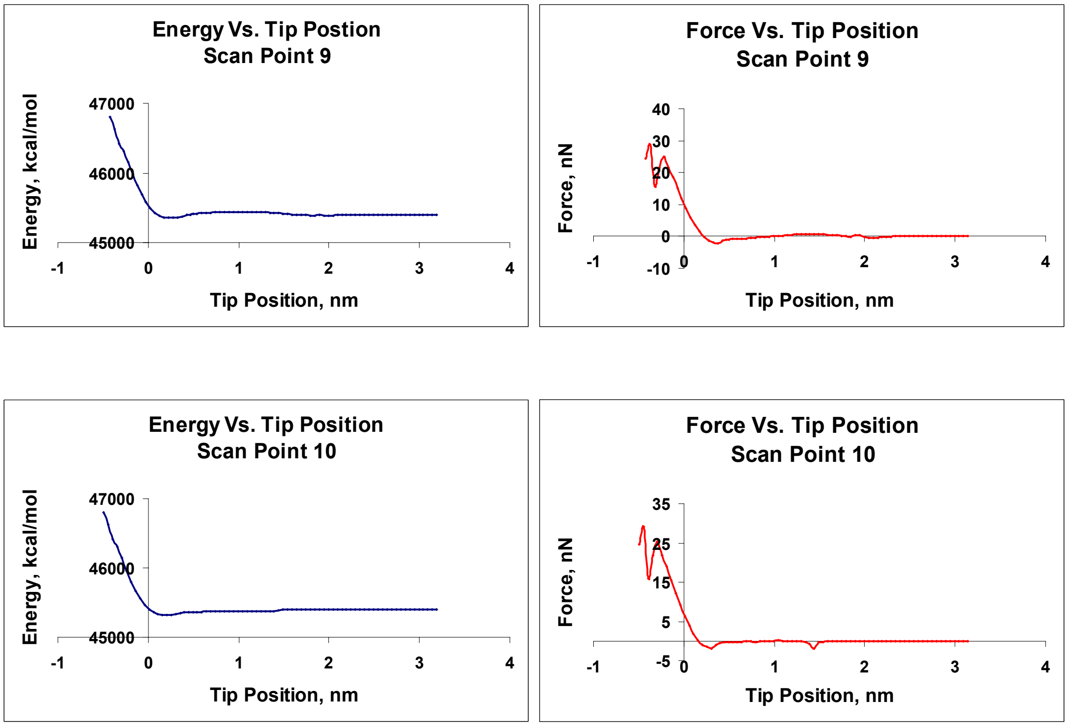

Figure S-1: Energy-distance and force-distance profiles generated for various probe positions, corresponding to the scan points in figure 2 of the manuscript.

Effect of thermal vibrations:

The tip-sample potentials and the corresponding force curves were constructed at zero kelvin to minimize the cost of the simulations. However, thermal vibration calculations at 300 K show that the potentials would not be significantly different at room temperature. The additional thermal energy would have the effect of lowering the energy barriers that the system needs to overcome in order for the probe to slip off the sample. This is only relevant for scan points 6, 7 and 8, for which the probe did not slip at the tip-sample forces present during tapping mode imaging. Only at much higher forces (~30 nN) did the probe slip off the sample nanotube at these points. The force and energy curves presented here show that the energy requirement to cause these points to slip is the same as that required to longitudinally compress the probe by one full nm, which is much greater than the available thermal energy. Our calculations show that the maximum horizontal displacement of any atom on the tip of the probe at 300 K is below 0.095 nm (less than 1.8% of the probe width), which would not significantly change the relative position of probe and sample. The amplitude of the vertical vibrations is less than 0.055 nm.

Characterization of SWNT deformation modes:

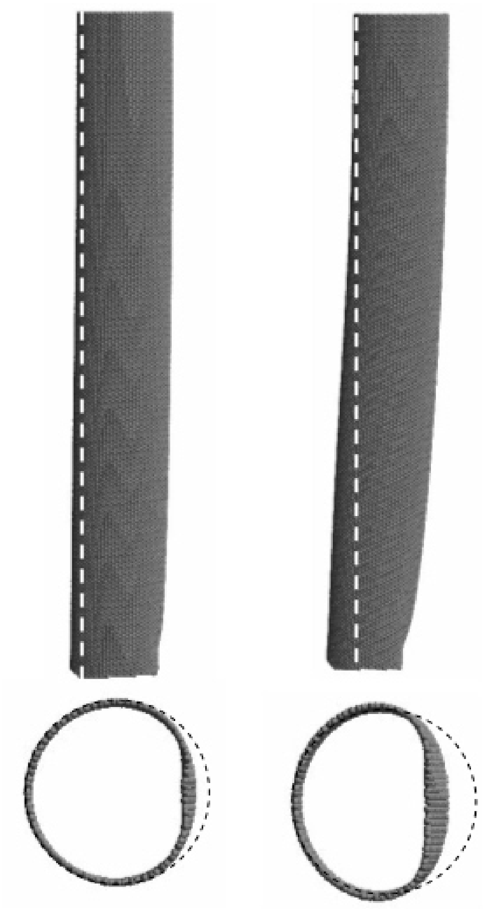

Scan Point 2 **Scan Point 5**

Figure S-2: Degree of probe bending shown for two extreme cases: scan point 2, the point on the scan where the 5.4 nm diameter probe nanotube first comes into contact with the sample nanotube, and scan point 5, the last point for which slipping occurred during the imaging simulation. The probe images have been rotated from their original tilted position to illustrate the amount of bending that the probe undergoes. The local deformation of the tip is also shown in the bottom pictures. The images show that both bending and local deformation contributes significantly to the reduction in the probe's effective resolution for this SWNT diameter.

Slipping of smaller SWNT probes: 2.2 nm diameter, 20 nm in length:

Figure S-3: The images from the simulation with the 2.2 nm diameter probe show that slipping also occurs for smaller probes, although it is primarily due to bending and not to local deformation, due to the higher radial stiffness for the thinner SWNT probes. In order to slip, the probe needed to displace laterally a distance of approximately 0.5 nm (22% of the sample diameter).

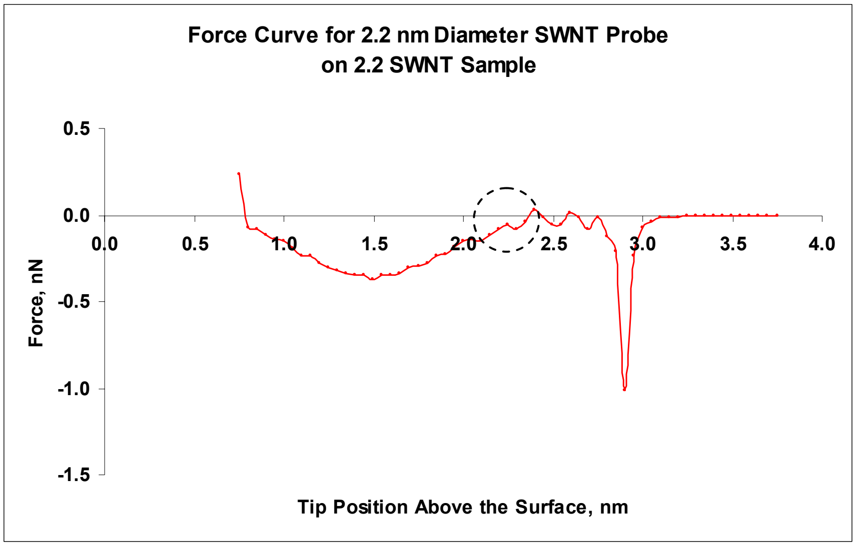

Figure S-4: Force curve for the 2.2 nm SNWT probe. The dashed circle shows the region where slipping occurs. As the graph shows, there is no significant force opposing the slipping motion of the probe. The negative peak in the force is due to snap-to-contact as the probe first approaches the sample.

Illustration of reversibility in SWNT probe-sample interaction:

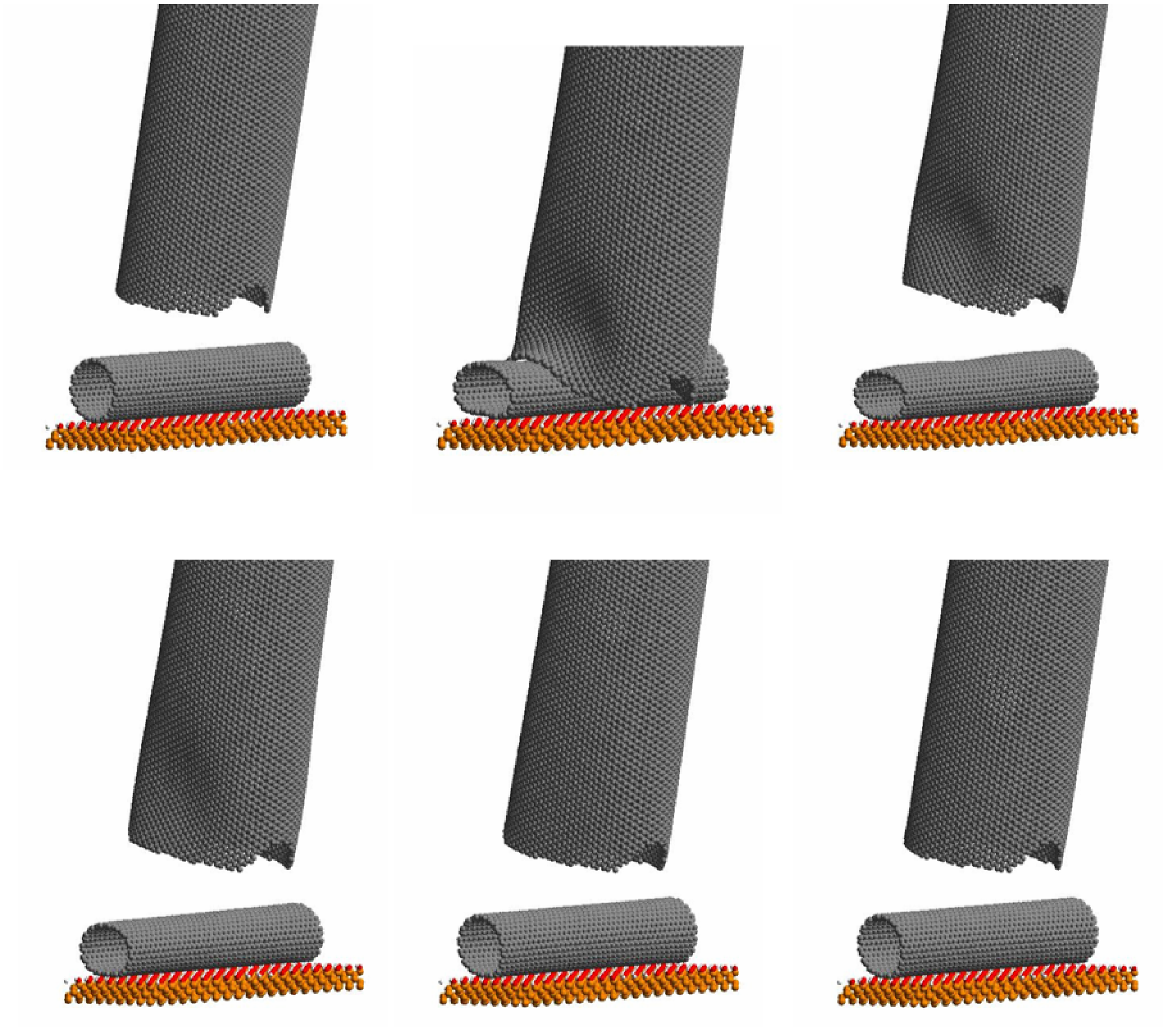

Figure S-5: Sequential images illustrating the reversible elastic nature of the deformation phenomenon. The top image on the left corresponds to the SWNT tip and sample before contact for scan point 6. The second image corresponds to the tip compressing the SWNT with a force of 33 nN (approximately twice the maximum tip-sample force observed during imaging). Images 3-6 correspond to intermediate geometry relaxation steps of the probe and sample after the probe has retracted. Note that the time required for geometry relaxation is on the order of 20 *ps,* one order of magnitude smaller than the integration time step used for AFM dynamics simulations (0.1 *ns*). This guarantees that the probe and sample are able to relax before the tip impacts the sample a second time.

References:

1. Musgrave, C.B., **1995.** PhD Dissertation Thesis: *"Molecular Mechanics and ab Initio Simulations of Silicon (111) Surface Reconstructions, Semiconductors and Semiconductor Superlattices, H Abstraction Tool for Nanotechnology, Polysilanes, and Growth of CVD Diamond"* California Institute of Technology.

2. Guo, Y.J. **1992.** PhD Dissertation Thesis: *"Molecular Simulations of Buckyball Fullerenes. Quantum Chemistry Studies on High Tc Superconductors"* California Institute of Technology.

3. Guo, Y.J.; Karasawan N.; Goddard W.A. III. *Nature,* **1991,** *351*, 6326.

4. Mayo, S.; Olafson, B.; Goddard, W. A. III. *J. Phys. Chem*. **1990**, 94, 8897.

Acknowledgements

My particular thanks to Pat Collier, Ian Shapiro, Maria Jose Esplandiu, and Santiago Solaris for being wonderful collaborators. Thanks also to Carol Garland for all of the TEM imaging used in this study. I gratefully acknowledge the help and advice of Jason Hafner who shared the pioneering nanotube fabrication techniques he developed without reservation. Funding for these efforts, provided by the Caltech President's Fund, JPL Research and Technology Development Program, Arrowhead Research and Pharmagenomix, is gratefully acknowledged.

References

---

[1] L. A. Wade, I. R. Shapiro, Z. Ma, S. R. Quake, and C. P. Collier, Correlating AFM Probe Morphology to Image Resolution for Single-Wall Carbon Nanotube Tips, Nano Lett., **2004**, 4, 725-731.

[2] I. R. Shapiro, S. D. Solares, M. J. Esplandiu, L. A Wade, W. A. Goddard and C. P. Collier, Influence of Elastic Deformation upon Single-Wall Carbon Nanotube AFM Probe Resolution, J. Phys. Chem. B, **2004,** *108*, 13613-13618.

[3] Method for Manufacturing Single Wall Carbon Nanotube Tips, US 7,211,795 B2, L.A. Wade, P. Collier, S. Quake, I. Shapiro, and Z. Ma issued May 1, 2007.

[4] Selective functionalization of carbon nanotube tips allowing fabrication of new classes of nanoscale sensing and manipulation tools, US 7,514,214, L.A. Wade, I.R. Shapiro, C. P. Collier, M.J. Esplandiu, V.G. Bittner and K.P. Giapis issued April 7, 2009.